Steel and Composite Structures, *Vol. 37, No. 1* (*2020*) *99-115*
DOI: https://doi.org/10.12989/scs.2020.37.1.099

Seismic analysis in pad concrete foundation reinforced by nanoparticles covered by smart layer utilizing plate higher order theory

Reza Taherifar[1], Seyed Alireza Zareei*[1], Mahmood Rabani Bidgoli[2] and Reza Kolahchi[3]

[1]*Department of Civil Engineering, Isfahan (Khorasgan) Branch, Islamic Azad University, Isfahan, Iran*
[2]*Department of Civil Engineering, Jasb Branch, Islamic Azad University, Jasb, Iran*
[3]*Institute of Research and Development, Duy Tan University, Da Nang 550000, Vietnam*

(*Received March 19, 2020, Revised September 20, 2020, Accepted September 26, 2020*)

Abstract. This article deals with the dynamic analysis in pad concrete foundation containing Silica nanoparticles (SiO_2) subject to seismic load. In order to control the foundation smartly, a piezoelectric layer covered the foundation. The weight of the building by a column on the foundation is assumed with an external force in the middle of the structure. The foundation is located in soil medium which is modeled by spring elements. The Mori-Tanaka law is utilized for calculating the equivalent mechanical characteristics of the concrete foundation. The Kevin-Voigt model is adopted to take into account the structural damping. The concrete structure is modeled by a thick plate and the governing equations are deduced using Hamilton's principle under the assumption of higher-order shear deformation theory (HSDT). The differential quadrature method (DQM) and the Newmark method are applied to obtain the seismic response. The effects of the applied voltage to the smart layer, agglomeration and volume percent of SiO_2 nanoparticles, damping of the structure, geometrical parameters and soil medium of the structure are assessed on the dynamic response. It has been demonstrated by the numerical results that by applying a negative voltage, the dynamic deflection is reduced significantly. Moreover, silica nanoparticles reduce the dynamic deflection of the concrete foundation.

Keywords: pad concrete foundation; dynamic defection; piezoelectric layer; soil medium; numerical method

1. Introduction

One of the important subjects for the design of buildings is resistance to seismic load. Recently, nanotechnology presents a new idea for the strength of the concrete structure using nanoparticles such as SiO_2. Due to the good mechanical properties of the nanoparticles, the compressive strength of the concrete can be improved.

The influence of nanoparticles on the concrete foam is studied by Hou *et al*. (2019). They found out that the stability of the prefabricated foams increased by the appropriate content of nanoparticles. Furthermore, the nanoparticles can enhance the strength of the concrete foam. Younis and Mustafa (2018) investigated the possibility of using nano-silica to improve the mechanical properties of agglomerated concrete. Moreover, they assessed the effect of nano SiO_2 on the water absorption of recycled aggregate concrete. Hosseini *et al*. (2009) assessed the influence of nano SiO_2 on the compressional strength of the recycled aggregated concrete. They experimentally determined the mechanical characteristics of the SiO_2 incorporated in aggregated concrete. A concreted pavement with nanoparticles is studied by Zhang and Yu (2011). The results indicated that the impact properties of the concrete with nanoparticle enhanced when the amount of the particles are smaller. They also declared that the flexural strength of concrete with nanoparticles has a linear relation with impact properties.

In the field of nanocomposite structures and numerical methods, Duc and Tung (2011) investigated the mechanical and thermal postbuckling of higher order shear deformable functionally graded plates on elastic foundations. Hieu and Tung (2020) studied the thermomechanical postbuckling of pressure-loaded CNT-reinforced composite cylindrical shells under tangential edge constraints and various temperature conditions. Analysis of laminated CNT reinforced functionally graded plates using the element-free kp-Ritz method is done by Lei *et al*. (2016). An overview of layerwise theories for composite laminates and structures is implemented by Liew *et al.* (2019). Long and Tung (2019) considered the Thermomechanical postbuckling behavior of CNT-reinforced composite sandwich plate models resting on elastic foundations with elastically restrained unloaded edges. Pan *et al.* (2019) modeled the geometrically nonlinear large deformation behaviors of matrix cracked hybrid composite deep shells containing CNTRC layers. Thermal buckling and postbuckling behaviour of functionally graded carbon-nanotube-reinforced composite plates resting on elastic foundations with tangential-edge restraints is studied by Tung (2017). Tung and Trang (2020) investigated the thermal postbuckling of shear deformable CNT-reinforced composite plates with tangentially restrained edges and temperature-dependent properties. Zhang (2017) proposed an element-free based IMLS-Ritz method for buckling analysis of nanocomposite plates of

*Corresponding author, Ph.D.
E-mail: alirezazareei89@gmail.com

Copyright © 2020 Techno-Press, Ltd.

ISSN: 1229-9367 (Print), 1598-6233 (Online)

polygonal planform. Zhang *et al*. (2016a) investigated an element-free analysis of CNT-reinforced composite plates with column supports and elastically restrained edges under large deformation. Postbuckling analysis of axially compressed CNT reinforced functionally graded composite plates resting on Pasternak foundations using an element-free approach is considered by Zhang and liew (2016a). Element-free geometrically nonlinear analysis of quadrilateral functionally graded material plates with internal column supports is investigated by Zhang and liew (2016b). Zhang *et al*. (2016c) investigated the postbuckling of carbon nanotube reinforced functionally graded plates with edges elastically restrained against translation and rotation under axial compression. The postbuckling analysis of bi-axially compressed laminated nanocomposite plates using the first-order shear deformation theory is investigated by Zhang *et al*. (2016d). Also, Zhang *et al*. (2016e) studied the Postbuckling behavior of bi-axially compressed arbitrarily straight-sided quadrilateral functionally graded material plates. In another research, Zhang *et al*. (2016f) analyzed the Geometrically nonlinear large deformation of triangular CNT-reinforced composite plates. Vibration of CNT-reinforced thick laminated composite plates based on Reddy's higher-order shear deformation theory is analyzed by Zhang and Selim (2017). Optimal shape control of CNT reinforced functionally graded composite plates using piezoelectric patches is done by Zhang *et al*. (2016g). aerothermoelastic properties and active flutter control of CNT reinforced functionally graded composite panels in supersonic airflow is computated by Zhang *et al*. (2016h). Zhang *et al*. (2017a) studied the dynamic responses of CNT-reinforced composite cylindrical shells under impact loads.

Due to the enhancement of the mechanical characteristics of the reinforced concrete with the nanoparticles, researchers focused on the dynamic analysis of the nano-reinforced concrete structures. Kargar and Bidgoli (2019) modeled the concrete foundation reinforced by the smart nanoparticles mathematically. The vibration response of the nano SiO_2 reinforced concrete foundation with a piezoelectric face-sheet on the structure is assessed. The results indicated that the frequency of the smart structure increased by applying negative voltage. The effect of blast load on the dynamic behavior of the concrete reinforced by SiO_2 is assessed in (2018; 2019). The numerical results demonstrated that as the silica particles increased the dynamic behavior of the nano-reinforced concrete decreased. The vibration response of the concrete beams with SiO_2 nanoparticles reinforcement is scrutinized by the Shokravi (2017). The effect of the silica nanoparticles agglomeration is considered adopting the Mori-Tanaka model. Golabchi *et al.* (2018) investigated the instability and dynamic response of the cylindrical shell reinforced by the silica nanoparticles. The results showed that the frequency decreased when the agglomeration of the silica nanoparticles is considered. The concrete pipes which are reinforced by the SiO_2 nanoparticles are assessed for the seismic behavior in (Maleki and Bidgoli 2018, Zarei *et al*. 2017, Motezaker and Kolahchi 2017). The conveying fluid pipes are subjected to the dynamic load and the influence of the silica nanoparticles on the structures examined. The results indicated that the displacement of the structure during the seismic load decreased as the silica nanoparticles used. Nouri (2018) studied the seismic behavior of the concrete pipes which are reinforced by the Fe_2O_3 nanoparticles on soil foundation. The soil foundation is modeled by the Winkler model Mori Tanaka approach is adopted to compute the effective elastic characteristics of the nanoparticles-reinforced concrete pipes. The seismic behavior of smart cylindrical shell conveying fluid with the carbon nanotube reinforcement is investigated by Zamani *et al.* (2017). They declared that dynamic displacement reduced as the piezoelectric layer is induced by negative voltage. The numerical and mathematical method was used to assessed the dynamic and seismic behavior of the concrete pipes in (Haghighi *et al*. 2018, Maleki *et al.* 2019). The conveying fluid pipes were immersed in the fluid and the effect of internal and external fluid assessed on the behavior. Hajmohammadi *et al.* (2018) studied the seismic behavior of the concrete pipes which were reinforced by the nano-fiber reinforced polymer. They analyzed the agglomeration effects and inner and outer fluid influence. A Mathematical model of concrete pipes using the carbon nanotubes as the reinforcements was presented by Nouri (2017). The vibration and stability analysis was conducted considering the magnetic field. Su *et al*. (2016) investigated the ultra-high performance concrete with nano-particles. They assessed the dynamic strength for both tensile and compressive loading. Concrete columns under buckling load analyzed by Safari Bilouei *et al*. (2016). The concrete columns were reinforced by nanofiber and the nanofiber effect was studied. TiO_2 nanoparticles were used as reinforcements in the concrete beam by Sharifi *et al*. (2018). They analyzed the dynamic response by subjecting the model to earthquake load and found out that dynamic deflection decreases. Analysis of critical fluid velocity and heat transfer in the nanocomposite pipes conveying nanofluid was presented by Fakhar *et al*. (2019).

Best of author's knowlegment, no reassert paper has been found for mathematical modelling and dynamic analysis of pad concrete foundation. This subject is a novel topic in civil engineering field. In the present study, a pad concrete foundation resting on the soli medium is modelled mathematically based on HSDT and its dynamic deflection induced by earthquake load is controlled by a piezoelectric layer. In addition, the structure is reinforced by SiO_2 nanoparticles and Kelvin-Voigt model is used for considering structural damping. Newmark and DQ methods are adopted to determine dynamic displacement. The influence of applied voltage to the smart layer, agglomeration and volume percent of silica nanoparticles, damping of the structure, geometrical parameters and soil medium are shown on the dynamic deflection.

2. Formulation

In Fig. 1, a pad concrete foundation is depicted with length, width, thickness of a, b and h_c, respectively. The structure is mixed by SiO_2 nanoparticles and covered by a

piezoelectric layer with a thickness of h_p. It is assumed that between smart layer and concrete foundation there is not any pore and the structure is continuous. In addition, the foundation is located at the soil medium which is modeled by the spring element. The weight of the building is applied through a column by an external load in the middle of the concrete foundation.

2.1 Kinematic relations

Based on the HSDT thick plate theory, the general displacements of the structure may be written as (Reddy 2002)

$$u_1(x,y,z,t)=u(x,y,t)+z\,\phi_x(x,y,t)+c_1 z^3\left(\phi_x+\frac{\partial w}{\partial x}\right), \tag{1a}$$

$$u_2(x,y,z,t)=v(x,y,t)+z\,\phi_y(x,y,t)+c_1 z^3\left(\phi_y+\frac{\partial w}{\partial y}\right), \tag{1b}$$

$$u_3(x,y,z,t)=w(x,y,t), \tag{1c}$$

The mid-plane displacements are u, v and w along the x, y, z directions, correspondingly; ϕ_x and ϕ_y present the rotational displacement about y and x directions, correspondingly. Utilizing the above relations, the relations between the strains and displacements are

$$\begin{pmatrix}\varepsilon_{xx}\\ \varepsilon_{yy}\\ \gamma_{xy}\end{pmatrix}=\begin{pmatrix}\varepsilon^0_{xx}\\ \varepsilon^0_{yy}\\ \gamma^0_{xy}\end{pmatrix}+z\begin{pmatrix}\varepsilon^1_{xx}\\ \varepsilon^1_{yy}\\ \gamma^1_{xy}\end{pmatrix}+z^3\begin{pmatrix}\varepsilon^3_{xx}\\ \varepsilon^3_{yy}\\ \gamma^3_{xy}\end{pmatrix}, \tag{2}$$

$$\begin{pmatrix}\gamma_{yz}\\ \gamma_{xz}\end{pmatrix}=\begin{pmatrix}\gamma^0_{yz}\\ \gamma^0_{xz}\end{pmatrix}+z^2\begin{pmatrix}\gamma^2_{yz}\\ \gamma^2_{xz}\end{pmatrix}, \tag{3}$$

where

$$\begin{pmatrix}\varepsilon^0_{xx}\\ \varepsilon^0_{yy}\\ \gamma^0_{xy}\end{pmatrix}=\begin{pmatrix}\dfrac{\partial u}{\partial x}\\ \dfrac{\partial v}{\partial y}\\ \dfrac{\partial u}{\partial y}+\dfrac{\partial v}{\partial x}\end{pmatrix},\quad \begin{pmatrix}\varepsilon^1_{xx}\\ \varepsilon^1_{yy}\\ \gamma^1_{xy}\end{pmatrix}=\begin{pmatrix}\dfrac{\partial \phi_x}{\partial x}\\ \dfrac{\partial \phi_y}{\partial y}\\ \dfrac{\partial \phi_x}{\partial y}+\dfrac{\partial \phi_y}{\partial x}\end{pmatrix}, \tag{4a}$$

$$\begin{pmatrix}\varepsilon^3_{xx}\\ \varepsilon^3_{yy}\\ \gamma^3_{xy}\end{pmatrix}=c_1\begin{pmatrix}\dfrac{\partial \phi_x}{\partial x}+\dfrac{\partial^2 w}{\partial x^2}\\ \dfrac{\partial \phi_y}{\partial y}+\dfrac{\partial^2 w}{\partial y^2}\\ \dfrac{\partial \phi_x}{\partial y}+\dfrac{\partial \phi_y}{\partial x}+2\dfrac{\partial^2 w}{\partial x\,\partial y}\end{pmatrix},$$

$$\begin{pmatrix}\gamma^0_{yz}\\ \gamma^0_{xz}\end{pmatrix}=\begin{pmatrix}\phi_y+\dfrac{\partial w}{\partial y}\\ \phi_x+\dfrac{\partial w}{\partial x}\end{pmatrix},\quad \begin{pmatrix}\gamma^2_{yz}\\ \gamma^2_{xz}\end{pmatrix}=c_2\begin{pmatrix}\phi_y+\dfrac{\partial w}{\partial y}\\ \phi_x+\dfrac{\partial w}{\partial x}\end{pmatrix}, \tag{4b}$$

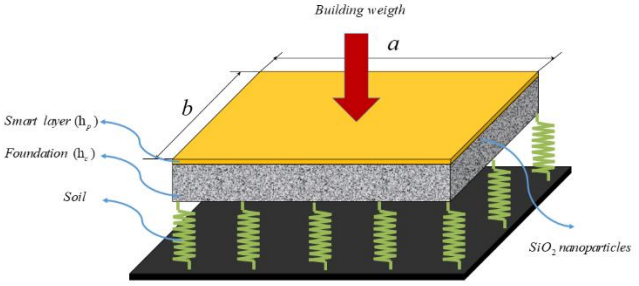

Fig. 1 A schematic configuration of pad concrete foundation containing nanoparticles covered by smart layer resting on soil medium

2.2 Basic equations of piezoelectric material

For the piezoelectric material, the stresses σ_{ij} and strains ε_{ij} are coupled by electric displacement D_i and by electric field E_i as follows (Tiersten 1969)

$$\begin{bmatrix}\sigma_{xx}\\ \sigma_{yy}\\ \sigma_{zz}\\ \tau_{yz}\\ \tau_{xz}\\ \tau_{xy}\end{bmatrix}=\begin{bmatrix}C_{11}&C_{12}&C_{13}&0&0&0\\ C_{12}&C_{22}&C_{23}&0&0&0\\ C_{13}&C_{23}&C_{33}&0&0&0\\ 0&0&0&C_{44}&0&0\\ 0&0&0&0&C_{55}&0\\ 0&0&0&0&0&C_{66}\end{bmatrix}\left\{\begin{bmatrix}\varepsilon_{xx}\\ \varepsilon_{yy}\\ \varepsilon_{zz}\\ \gamma_{yz}\\ \gamma_{xz}\\ \gamma_{xy}\end{bmatrix}\right\}$$
$$-\begin{bmatrix}0&0&e_{31}\\ 0&0&e_{32}\\ 0&0&e_{33}\\ 0&e_{24}&0\\ e_{15}&0&0\\ 0&0&0\end{bmatrix}\begin{Bmatrix}E_x\\ E_y\\ E_z\end{Bmatrix} \tag{5}$$

$$\begin{bmatrix}D_x\\ D_y\\ D_z\end{bmatrix}=\begin{bmatrix}0&0&0&0&e_{15}&0\\ 0&0&0&e_{24}&0&0\\ e_{31}&e_{31}&e_{33}&0&0&0\end{bmatrix}\left\{\begin{bmatrix}\varepsilon_{xx}\\ \varepsilon_{yy}\\ \varepsilon_{zz}\\ \gamma_{yz}\\ \gamma_{xz}\\ \gamma_{xy}\end{bmatrix}\right\}$$
$$+\begin{bmatrix}\in_{11}&0&0\\ 0&\in_{22}&0\\ 0&0&\in_{33}\end{bmatrix}\begin{Bmatrix}E_x\\ E_y\\ E_z\end{Bmatrix} \tag{6}$$

The elastic, dielectric and piezoelectric constants are indicated by C_{ij}, $\in_{ij}$ and e_{ij} respectively.

The electric field can be determined respect to the electric potential (Φ)

$$E_k=-\nabla\Phi, \tag{7}$$

Where the electric potential is considered consists of a linear variation and half-cosine (the Maxwell equation are satisfied) as

$$\Phi(x,y,z,t)=-\cos(\frac{\pi z}{h})\varphi(x,y,t)+\frac{2V_0 z}{h}, \tag{8}$$

where $\varphi(x,y,t)$ is the electric potential with satisfying the boundary conditions related to electric; V_0 is the external voltage. Based on Eqs. (2)-(5), the stress equations of the smart layer may be given as (Tiersten 1969, Kolahchi *et al*. 2016)

$$\sigma_{xx}^{p}=C_{11}\varepsilon_{xx}+C_{12}\varepsilon_{yy}+e_{31}\left(\frac{\pi}{h}\sin\left(\frac{\pi z}{h}\right)\varphi+\frac{2V_0}{h}\right), \tag{9}$$

$$\sigma_{yy}^{p}=C_{12}\varepsilon_{xx}+C_{22}\varepsilon_{yy}+e_{32}\left(\frac{\pi}{h}\sin\left(\frac{\pi z}{h}\right)\varphi+\frac{2V_0}{h}\right), \tag{10}$$

$$\tau_{yz}^{p}=C_{44}\gamma_{yz}-e_{15}\left(\cos\left(\frac{\pi z}{h}\right)\frac{\partial\varphi}{\partial y}\right), \tag{11}$$

$$\tau_{xz}^{p}=C_{55}\gamma_{zx}-e_{24}\left(\cos\left(\frac{\pi z}{h}\right)\frac{\partial\varphi}{\partial x}\right), \tag{12}$$

$$\tau_{xy}^{p}=C_{66}\gamma_{xy}, \tag{13}$$

Utilizing Eqs. (2)-(4) and (6), the electric displacement equations of the piezoelectric layer are

$$D_x=e_{15}\gamma_{xz}+\in_{11}\left(\cos\left(\frac{\pi z}{h}\right)\frac{\partial\varphi}{\partial y}\right), \tag{14}$$

$$D_y=e_{24}\gamma_{zy}+\in_{22}\left(\cos\left(\frac{\pi z}{h}\right)\frac{\partial\varphi}{\partial y}\right), \tag{15}$$

$$D_z=e_{31}\varepsilon_{xx}+e_{32}\varepsilon_{yy}-\in_{33}\left(\frac{\pi}{h}\sin\left(\frac{\pi z}{h}\right)\varphi+\frac{2V_0}{h}\right). \tag{16}$$

2.3 Basic equations of concrete foundation containing nanoparticles

For the pad concrete foundation, the stress relations can be given by neglecting piezoelectric constants of Eqs. (9)-(13) as

$$\sigma_{xx}^{c}=\underbrace{\frac{E}{1-\nu^2}}_{Q_{11}}\varepsilon_{xx}+\underbrace{\frac{E\nu}{1-\nu^2}}_{Q_{12}}\varepsilon_{yy}, \tag{17}$$

$$\sigma_{yy}^{c}=\underbrace{\frac{E\nu}{1-\nu^2}}_{Q_{12}}\varepsilon_{xx}+\underbrace{\frac{E}{1-\nu^2}}_{Q_{22}}\varepsilon_{yy}, \tag{18}$$

$$\tau_{yz}^{c}=\underbrace{\frac{E}{2(1+\nu)}}_{Q_{44}}\gamma_{yz}, \tag{19}$$

$$\tau_{xz}^{c}=\underbrace{\frac{E}{2(1+\nu)}}_{Q_{55}}\gamma_{zx}, \tag{20}$$

$$\tau_{xy}^{c}=\underbrace{\frac{E}{2(1+\nu)}}_{Q_{66}}\gamma_{xy}, \tag{21}$$

where the modulus of elasticity (E) and Poisson's ratio (ν) based on the Mori-Tanaka model (Shi and Feng, 20 04) may be given as

$$E=\frac{9KG}{3K+G}, \tag{22}$$

$$\nu=\frac{3K-2G}{6K+2G}. \tag{23}$$

in which the equivalent shear modulus (G) and bulk mod ulus (K) are presented in Appendix A.

2.4 Energy method

The potential energy related to pad concrete foundation with a smart layer can be expressed as

$$U=\frac{1}{2}\int\begin{pmatrix}\sigma_{xx}^{c}\varepsilon_{xx}+\sigma_{yy}^{c}\varepsilon_{yy}+\tau_{xz}^{c}\gamma_{xz}+\tau_{yz}^{c}\gamma_{yz}\\+\tau_{xy}^{c}\gamma_{xy}+\sigma_{xx}^{p}\varepsilon_{xx}+\sigma_{yy}^{p}\varepsilon_{yy}+\tau_{xz}^{p}\gamma_{xz}\\+\tau_{yz}^{p}\gamma_{yz}+\tau_{xy}^{p}\gamma_{xy}\\-D_x E_x-D_y E_y-D_z E_z\end{pmatrix}dV, \tag{24}$$

Substituting Eqs. (2)-(8) into Eq. (24) yields

$$\begin{aligned}U=&\frac{1}{2}\int\left(N_{xx}\left(\frac{\partial u}{\partial x}\right)+N_{yy}\left(\frac{\partial v}{\partial y}\right)+Q_{yy}\left(\frac{\partial w}{\partial y}+\phi_y\right)\right.\\&+Q_{xx}\left(\frac{\partial w}{\partial x}+\phi_x\right)+N_{xy}\left(\frac{\partial v}{\partial x}+\frac{\partial u}{\partial y}\right)+M_{xx}\frac{\partial\phi_x}{\partial x}\\&+M_{yy}\frac{\partial\phi_y}{\partial y}+M_{xy}\left(\frac{\partial\phi_x}{\partial y}+\frac{\partial\phi_y}{\partial x}\right)+K_{yy}\left(c_2\left(\phi_y+\frac{\partial w}{\partial y}\right)\right)\\&+K_{xx}\left(c_2\left(\phi_x+\frac{\partial w}{\partial x}\right)\right)+P_{xx}\left(c_1\left(\frac{\partial\phi_x}{\partial x}+\frac{\partial^2 w}{\partial x^2}\right)\right)\\&\left.+P_{yy}\left(c_1\left(\frac{\partial\phi_y}{\partial y}+\frac{\partial^2 w}{\partial y^2}\right)\right)+P_{xy}\left(\frac{\partial\phi_y}{\partial x}+\frac{\partial\phi_x}{\partial y}+2\frac{\partial^2 w}{\partial x\,\partial y}\right)\right)dA\\&+\int_{-h/2}^{h/2+h_p}\int_0^{2\pi}\int_0^{L}-D_x\left[\cos\left(\frac{\pi z}{h}\right)\frac{\partial\varphi}{\partial x}\right]-D_y\left[\cos\left(\frac{\pi z}{h}\right)\frac{\partial\varphi}{\partial y}\right]\\&\left.-D_z\left[-\frac{\pi}{h}\sin\left(\frac{\pi z}{h}\right)\varphi-\frac{2V_0}{h}\right]\right\}dx\,dy\,dz,\end{aligned} \tag{25}$$

where the resultant may be given as

$$\begin{Bmatrix}N_{xx}\\N_{yy}\\N_{xy}\end{Bmatrix}=\int_{-\frac{h_c}{2}}^{\frac{h_c}{2}}\begin{Bmatrix}\sigma_{xx}^{c}\\\sigma_{yy}^{c}\\\tau_{xy}^{c}\end{Bmatrix}dz+\int_{\frac{h_c}{2}}^{\frac{h_c}{2}+h_p}\begin{Bmatrix}\sigma_{xx}^{p}\\\sigma_{yy}^{p}\\\tau_{xy}^{p}\end{Bmatrix}dz \tag{26}$$

$$\begin{Bmatrix}Q_x\\Q_y\end{Bmatrix}=\int_{-\frac{h_c}{2}}^{\frac{h_c}{2}}\begin{Bmatrix}\tau_{xz}^{c}\\\tau_{yz}^{c}\end{Bmatrix}dz+\int_{-\frac{h_c}{2}}^{\frac{h_c}{2}+h_p}\begin{Bmatrix}\tau_{xz}^{p}\\\tau_{yz}^{p}\end{Bmatrix}dz, \tag{27}$$

$$\begin{Bmatrix}M_{xx}\\M_{yy}\\M_{xy}\end{Bmatrix}=\int_{-\frac{h_c}{2}}^{\frac{h_c}{2}}\begin{Bmatrix}\sigma_{xx}^{c}\\\sigma_{yy}^{c}\\\tau_{xy}^{c}\end{Bmatrix}z^2dz+\int_{\frac{h_c}{2}}^{\frac{h_c}{2}+h_p}\begin{Bmatrix}\sigma_{xx}^{p}\\\sigma_{yy}^{p}\\\tau_{xy}^{p}\end{Bmatrix}z^2dz, \tag{28}$$

$$\begin{Bmatrix} P_{xx} \\ P_{yy} \\ P_{xy} \end{Bmatrix} = \int_{-\frac{h_c}{2}}^{\frac{h_c}{2}} \begin{Bmatrix} \sigma_{xx}^c \\ \sigma_{yy}^c \\ \tau_{xy}^c \end{Bmatrix} z^3 dz + \int_{\frac{h_c}{2}}^{\frac{h_c}{2}+h_p} \begin{Bmatrix} \sigma_{xx}^p \\ \sigma_{yy}^p \\ \tau_{xy}^p \end{Bmatrix} z^3 dz, \tag{29}$$

$$\begin{Bmatrix} K_x \\ K_y \end{Bmatrix} = \int_{-\frac{h_c}{2}}^{\frac{h_c}{2}} \begin{Bmatrix} \tau_{xz}^c \\ \tau_{yz}^c \end{Bmatrix} z^2 dz + \int_{-\frac{h_c}{2}}^{\frac{h_c}{2}+h_p} \begin{Bmatrix} \tau_{xz}^p \\ \tau_{yz}^p \end{Bmatrix} z^2 dz, \tag{30}$$

The kinetic energy related to the smart concrete structure is

$$K = \frac{\left(\rho^c + \rho^p\right)}{2} \int \left(\dot{u}_1^2 + \dot{u}_2^2 + \dot{u}_3^2\right) dV, \tag{31}$$

where ρ^c and ρ^p are density of concrete and smart layer, respectively.

The external work due to soil medium, lateral load of building weight and earthquake load can be given as

$$W_e = \int_0^{2\pi} \int_0^L \begin{bmatrix} \mathrm{ma}_x u + \mathrm{ma}_y v + \\ \left(-K_s w + F\delta(\mathrm{x}-a/2)(y-b/2) + \mathrm{ma}_z\right) w \end{bmatrix} dA, \tag{32}$$

where K_s is soil spring constant; F is the force of building weight; m is the weight of the structure; a is the acceleration of earthquake.

2.5 Motion equations

Hamilton's principle is adopted to infer the governing equations

$$\int_0^t (\delta U - \delta K - \delta W_e) dt = 0. \tag{33}$$

Replacing the Eqs. (25), (31) and (32) into Eq. (33) yields

$$\delta u: \frac{\partial N_{xx}}{\partial x} + \frac{\partial N_{xy}}{\partial y} = I_0 \frac{\partial^2 u}{\partial t^2} + J_1 \frac{\partial^2 \phi_x}{\partial t^2} - \frac{4I_3}{h^2} \frac{\partial^3 w}{\partial t^2 \partial x} + \mathrm{ma}_x, \tag{34}$$

$$\delta v: \frac{\partial N_{xy}}{\partial x} + \frac{\partial N_{yy}}{\partial y} = I_0 \frac{\partial^2 v}{\partial t^2} + J_1 \frac{\partial^2 \phi_y}{\partial t^2} - \frac{4I_3}{h^2} \frac{\partial^3 w}{\partial t^2 \partial y} + \mathrm{ma}_y, \tag{35}$$

$$\begin{aligned} &\delta w: \frac{\partial Q_{xx}}{\partial x} + \frac{\partial Q_{yy}}{\partial y} + c_2 \left(\frac{\partial K_{xx}}{\partial x} + \frac{\partial K_{yy}}{\partial y} \right) + N_{xx} \frac{\partial^2 w}{\partial x^2} + N_{yy} \frac{\partial^2 w}{\partial y^2} \\ &- c_1 \left(\frac{\partial^2 P_{xx}}{\partial x^2} + 2\frac{\partial^2 P_{xy}}{\partial x \partial y} + \frac{\partial^2 P_{yy}}{\partial y^2} \right) - F\delta(\mathrm{x}-a/2)(y-b/2) \\ &- K_s w = I_0 \frac{\partial^2 w}{\partial t^2} - \left(\frac{4}{3h^2}\right)^2 I_6 \left(\frac{\partial^4 w}{\partial x^2 \partial t^2} + \frac{\partial^4 w}{\partial y^2 \partial t^2} \right) \\ &+ \frac{4}{3h^2} \left(J_4 \left(\frac{\partial^3 \phi_x}{\partial t^2 \partial x} + \frac{\partial^3 \phi_\varepsilon}{\partial t^2 \partial y} \right) + I_3 \frac{\partial^3 v}{\partial t^2 \partial y} + I_3 \frac{\partial^3 u}{\partial t^2 \partial x} \right) + \mathrm{ma}_z, \end{aligned} \tag{36}$$

$$\begin{aligned} &\delta\phi_x: \frac{\partial M_{xx}}{\partial x} + \frac{\partial M_{xy}}{\partial y} + c_1 \left(\frac{\partial P_{xx}}{\partial x} + \frac{\partial P_{xy}}{\partial y} \right) - Q_{xx} - c_2 K_{xx} = \\ &J_1 \frac{\partial^2 u}{\partial t^2} + K_2 \frac{\partial^2 \phi_x}{\partial t^2} - J_4 \frac{4}{3h^2} \frac{\partial^3 w}{\partial t^2 \partial x} - \left(\frac{h}{2} + \frac{c_1 h^3}{8} \right) \mathrm{ma}_x, \end{aligned} \tag{37}$$

$$\begin{aligned} &\delta\phi_y: \frac{\partial M_{xy}}{\partial x} + \frac{\partial M_{yy}}{\partial y} + c_1 \left(\frac{\partial P_{xy}}{\partial x} + \frac{\partial P_{yy}}{\partial y} \right) - Q_{yy} - c_2 K_{yy} \\ &= J_1 \frac{\partial^2 v}{\partial t^2} + K_2 \frac{\partial^2 \phi_y}{\partial t^2} - \frac{4}{3h^2} J_4 \frac{\partial^3 w}{\partial t^2 \partial y} - \left(\frac{h}{2} + \frac{c_1 h^3}{8} \right) \mathrm{ma}_y, \end{aligned} \tag{38}$$

$$\begin{aligned} &\delta\varphi: \int_{-h/2}^{h/2} \left\{ \cos\left(\frac{\pi z}{h}\right) \left[\frac{\partial D_x}{\partial x} \right] + \cos\left(\frac{\pi z}{h}\right) \left[\frac{\partial D_y}{\partial y} \right] \right. \\ &\left. + \frac{\pi}{h} \sin\left(\frac{\pi z}{h}\right) [D_z] \right\} dz = 0 \end{aligned} \tag{39}$$

where the moment of inertias are

$$I_i = \int_{-h_c/2}^{h_c/2} \rho^c z^i dz + \int_{h_c/2}^{h_c/2+h_p} \rho^p z^i dz, \tag{40}$$

$$J_i = I_i - \frac{4}{3h^2} I_{i+2} \qquad (i = 1,4), \tag{41}$$

$$K_2 = I_2 - \frac{8}{3h^2} I_4 + \left(\frac{4}{3h^2} \right)^2 I_6, \tag{42}$$

Substituting Eqs. (2)-(6) into Eqs. (26)-(28), the stress resultants may be expressed as

$$\begin{aligned} N_{xx} &= A_{11} \frac{\partial u}{\partial x} + A_{12} \frac{\partial v}{\partial y} + A_{16} \left(\frac{\partial u}{\partial y} + \frac{\partial v}{\partial x} \right) \\ &+ B_{11} \frac{\partial \varphi_x}{\partial x} + B_{12} \frac{\partial \varphi_y}{\partial y} + B_{16} \left(\frac{\partial \phi_x}{\partial y} + \frac{\partial \phi_y}{\partial x} \right) \\ &+ E_{11} c_1 \left(\frac{\partial \varphi_x}{\partial x} + \frac{\partial^2 w}{\partial x^2} \right) + E_{12} c_1 \left(\frac{\partial \phi_y}{\partial y} + \frac{\partial^2 w}{\partial y^2} \right) \\ &+ E_{16} c_1 \left(\frac{\partial \phi_y}{\partial x} + \frac{\partial \phi_x}{\partial y} + 2\frac{\partial^2 w}{\partial x \partial y} \right), \\ N_{yy} &= A_{12} \frac{\partial u}{\partial x} + A_{22} \frac{\partial v}{\partial y} + A_{26} \left(\frac{\partial u}{\partial y} + \frac{\partial v}{\partial x} \right) \\ &+ B_{12} \frac{\partial \phi_x}{\partial x} + B_{22} \frac{\partial \phi_y}{\partial y} + B_{26} \left(\frac{\partial \phi_x}{\partial y} + \frac{\partial \phi_y}{\partial x} \right) \\ &+ E_{12} c_1 \left(\frac{\partial \phi_x}{\partial x} + \frac{\partial^2 w}{\partial x^2} \right) + E_{22} c_1 \left(\frac{\partial \phi_y}{\partial y} + \frac{\partial^2 w}{\partial y^2} \right) \\ &+ E_{26} c_1 \left(\frac{\partial \phi_y}{\partial x} + \frac{\partial \phi_x}{\partial y} + 2\frac{\partial^2 w}{\partial x \partial y} \right), \\ N_{xy} &= A_{16} \frac{\partial u}{\partial x} + A_{26} \frac{\partial v}{\partial y} + A_{66} \left(\frac{\partial u}{\partial y} + \frac{\partial v}{\partial x} \right) \\ &+ B_{16} \frac{\partial \phi_x}{\partial x} + B_{26} \frac{\partial \phi_y}{\partial y} + B_{66} \left(\frac{\partial \phi_x}{\partial y} + \frac{\partial \phi_y}{\partial x} \right) \\ &+ E_{16} c_1 \left(\frac{\partial \phi_x}{\partial x} + \frac{\partial^2 w}{\partial x^2} \right) + E_{26} c_1 \left(\frac{\partial \phi_y}{\partial y} + \frac{\partial^2 w}{\partial y^2} \right) \\ &+ E_{66} c_1 \left(\frac{\partial \phi_y}{\partial x} + \frac{\partial \phi_x}{\partial y} + 2\frac{\partial^2 w}{\partial x \partial y} \right), \end{aligned} \tag{43}$$

$$\begin{aligned} M_{xx} &= B_{11} \frac{\partial u}{\partial x} + B_{12} \frac{\partial v}{\partial y} + B_{16} \left(\frac{\partial u}{\partial y} + \frac{\partial v}{\partial x} \right) \\ &+ D_{11} \frac{\partial \phi_x}{\partial x} + D_{12} \frac{\partial \phi_y}{\partial y} + D_{16} \left(\frac{\partial \phi_x}{\partial y} + \frac{\partial \phi_y}{\partial x} \right) \\ &+ F_{11} c_1 \left(\frac{\partial \phi_x}{\partial x} + \frac{\partial^2 w}{\partial x^2} \right) + F_{12} c_1 \left(\frac{\partial \phi_y}{\partial y} + \frac{\partial^2 w}{\partial y^2} \right) \\ &+ F_{16} c_1 \left(\frac{\partial \phi_y}{\partial x} + \frac{\partial \phi_x}{\partial y} + 2\frac{\partial^2 w}{\partial x \partial y} \right), \\ M_{yy} &= B_{12} \frac{\partial u}{\partial x} + B_{22} \frac{\partial v}{\partial y} + B_{26} \left(\frac{\partial u}{\partial y} + \frac{\partial v}{\partial x} \right) \\ &+ D_{12} \frac{\partial \phi_x}{\partial x} + D_{22} \frac{\partial \phi_y}{\partial y} + D_{26} \left(\frac{\partial \phi_x}{\partial y} + \frac{\partial \phi_y}{\partial x} \right) \\ &+ F_{12} c_1 \left(\frac{\partial \phi_x}{\partial x} + \frac{\partial^2 w}{\partial x^2} \right) + F_{22} c_1 \left(\frac{\partial \phi_y}{\partial y} + \frac{\partial^2 w}{\partial y^2} \right) \\ &+ F_{26} c_1 \left(\frac{\partial \phi_y}{\partial x} + \frac{\partial \phi_x}{\partial y} + 2\frac{\partial^2 w}{\partial x \partial y} \right), \\ M_{xy} &= B_{16} \frac{\partial u}{\partial x} + B_{26} \frac{\partial v}{\partial y} + B_{66} \left(\frac{\partial u}{\partial y} + \frac{\partial v}{\partial x} \right) \\ &+ D_{16} \frac{\partial \phi_x}{\partial x} + D_{26} \frac{\partial \phi_y}{\partial y} + D_{66} \left(\frac{\partial \phi_x}{\partial y} + \frac{\partial \phi_y}{\partial x} \right) \\ &+ F_{16} c_1 \left(\frac{\partial \phi_x}{\partial x} + \frac{\partial^2 w}{\partial x^2} \right) + F_{26} c_1 \left(\frac{\partial \phi_y}{\partial y} + \frac{\partial^2 w}{\partial y^2} \right) \\ &+ F_{66} c_1 \left(\frac{\partial \phi_y}{\partial x} + \frac{\partial \phi_x}{\partial y} + 2\frac{\partial^2 w}{\partial x \partial y} \right), \end{aligned} \tag{44}$$

$$
\begin{aligned}
P_{xx} &= E_{11}\frac{\partial u}{\partial x}+E_{12}\frac{\partial v}{\partial y}+E_{16}\left(\frac{\partial u}{\partial y}+\frac{\partial v}{\partial x}\right)\\
&+F_{11}\frac{\partial \phi_x}{\partial x}+F_{12}\frac{\partial \phi_y}{\partial y}+F_{16}\left(\frac{\partial \phi_x}{\partial y}+\frac{\partial \phi_y}{\partial x}\right)\\
&+H_{11}c_1\left(\frac{\partial \phi_x}{\partial x}+\frac{\partial^2 w}{\partial x^2}\right)+H_{12}c_1\left(\frac{\partial \phi_y}{\partial y}+\frac{\partial^2 w}{\partial y^2}\right)\\
&+H_{16}c_1\left(\frac{\partial \phi_y}{\partial x}+\frac{\partial \phi_x}{\partial y}+2\frac{\partial^2 w}{\partial x\,\partial y}\right),\\
P_{yy} &= E_{12}\frac{\partial u}{\partial x}+E_{22}\frac{\partial v}{\partial y}+E_{26}\left(\frac{\partial u}{\partial y}+\frac{\partial v}{\partial x}\right)\\
&+F_{12}\frac{\partial \phi_x}{\partial x}+F_{22}\frac{\partial \phi_y}{\partial y}+F_{26}\left(\frac{\partial \phi_x}{\partial y}+\frac{\partial \phi_y}{\partial x}\right)\\
&+H_{12}c_1\left(\frac{\partial \phi_x}{\partial x}+\frac{\partial^2 w}{\partial x^2}\right)+H_{22}c_1\left(\frac{\partial \phi_y}{\partial y}+\frac{\partial^2 w}{\partial y^2}\right)\\
&+H_{26}c_1\left(\frac{\partial \phi_y}{\partial x}+\frac{\partial \phi_x}{\partial y}+2\frac{\partial^2 w}{\partial x\,\partial y}\right),\\
P_{xy} &= E_{16}\frac{\partial u}{\partial x}+E_{26}\frac{\partial v}{\partial y}+E_{66}\left(\frac{\partial u}{\partial y}+\frac{\partial v}{\partial x}\right)\\
&+F_{16}\frac{\partial \phi_x}{\partial x}+F_{26}\frac{\partial \phi_y}{\partial y}+F_{66}\left(\frac{\partial \phi_x}{\partial y}+\frac{\partial \phi_y}{\partial x}\right)\\
&+H_{16}c_1\left(\frac{\partial \phi_x}{\partial x}+\frac{\partial^2 w}{\partial x^2}\right)+H_{26}c_1\left(\frac{\partial \phi_y}{\partial y}+\frac{\partial^2 w}{\partial y^2}\right)\\
&+H_{66}c_1\left(\frac{\partial \phi_y}{\partial x}+\frac{\partial \phi_x}{\partial y}+2\frac{\partial^2 w}{\partial x\,\partial y}\right),
\end{aligned}
\tag{45}
$$

$$
\begin{aligned}
Q_{xx} &= A_{55}\left(\frac{\partial w}{\partial x}+\phi_x\right)+A_{45}\left(\frac{\partial w}{\partial y}+\phi_y\right)\\
&+D_{55}c_2\left(\phi_x+\frac{\partial w}{\partial x}\right)+D_{45}c_2\left(\frac{\partial w}{\partial y}+\phi_y\right),\\
Q_{yy} &= A_{45}\left(\frac{\partial w}{\partial y}+\phi_y\right)+A_{44}\left(\frac{\partial w}{\partial y}+\phi_y\right)\\
&+D_{45}c_2\left(\phi_y+\frac{\partial w}{\partial y}\right)+D_{44}c_2\left(\frac{\partial w}{\partial y}+\phi_y\right),
\end{aligned}
\tag{46}
$$

$$
K_{xx} = D_{55}\left(\phi_x+\frac{\partial w}{\partial x}\right)+D_{45}\left(\phi_y+\frac{\partial w}{\partial y}\right)+F_{55}c_2\left(\phi_x+\frac{\partial w}{\partial x}\right)+F_{45}c_2\left(\phi_y+\frac{\partial w}{\partial y}\right),
$$

$$
K_{yy} = D_{45}\left(\phi_x+\frac{\partial w}{\partial x}\right)+D_{44}\left(\phi_y+\frac{\partial w}{\partial y}\right)+F_{45}c_2\left(\phi_x+\frac{\partial w}{\partial x}\right)+F_{44}c_2\left(\phi_y+\frac{\partial w}{\partial y}\right),
\tag{47}
$$

$$
B_{ij} = \left(1+g\frac{\partial}{\partial t}\right)\left[\int_{-h_c/2}^{h_c/2} Q_{11}z^2dz+\int_{-h_c/2}^{h_c/2+h_p} C_{11}z^2dz\right],
\tag{49}
$$

$$
D_{ij} = \left(1+g\frac{\partial}{\partial t}\right)\left[\int_{-h_c/2}^{h_c/2} Q_{11}z^2dz+\int_{-h_c/2}^{h_c/2+h_p} C_{11}z^2dz\right],
\tag{50}
$$

$$
E_{ij} = \left(1+g\frac{\partial}{\partial t}\right)\left[\int_{-h_c/2}^{h_c/2} Q_{11}z^3dz+\int_{-h_c/2}^{h_c/2+h_p} C_{11}z^3dz\right],
\tag{51}
$$

$$
F_{ij} = \left(1+g\frac{\partial}{\partial t}\right)\left[\int_{-h_c/2}^{h_c/2} Q_{11}z^4dz+\int_{-h_c/2}^{h_c/2+h_p} C_{11}z^4dz\right],
\tag{52}
$$

$$
H_{ij} = \left(1+g\frac{\partial}{\partial t}\right)\left[\int_{-h_c/2}^{h_c/2} Q_{11}z^6dz+\int_{-h_c/2}^{h_c/2+h_p} C_{11}z^6dz\right],
\tag{53}
$$

where g is the damping parameter of the structure. Replacing the Eqs. (43) to (47) into Eqs. (34) to (39), the motion equations are expanded in terms of displacements as written in Appendix B.

3. Numerical method

Utilizing DQM, the differential motion equations may be turned into algebraic equations applying weighting coefficients. Hence, the derivative of a function with respect to x and y is written as (Kolahchi *et al*. 2016)

$$
\frac{d^n f_x(x_i,y_j)}{dx^n}=\sum_{k=1}^{N_x}A_{ik}^{(n)}f(x_k,y_j)\quad n=1,...,N_x-1.
\tag{54}
$$

$$
\frac{d^m f_y(x_i,y_j)}{dy^m}=\sum_{l=1}^{N_y}B_{jl}^{(m)}f(x_i,y_l)\quad m=1,...,N_y-1.
\tag{55}
$$

$$
\frac{d^{n+m} f_{xy}(x_i,y_j)}{dx^n dy^m}=\sum_{k=1}^{N_x}\sum_{l=1}^{N_y}A_{ik}^{(n)}B_{jl}^{(m)}f(x_k,y_l).
\tag{56}
$$

In which the weighting coefficients may be given as

$$
A_{ij}^{(1)}=\begin{cases}
\dfrac{\prod_{\substack{j=1\\ j\neq i}}^{N_x}(x_i-x_j)}{(x_i-x_j)\prod_{\substack{j=1\\ j\neq i}}^{N_x}(x_i-x_j)} & \text{for}\quad i,j=1,2,...,N_x,\quad i\neq j\\
-\sum_{\substack{j=1\\ i\neq j}}^{N_x}A_{ij}^{(1)} & \text{for}\quad i,j=1,2,...,N_x\quad i=j
\end{cases}
\tag{57}
$$

$$
B_{ij}^{(1)}=\begin{cases}
\dfrac{\prod_{\substack{j=1\\ j\neq i}}^{N_y}(y_i-y_j)}{(y_i-y_j)\prod_{\substack{j=1\\ j\neq i}}^{N_y}(y_i-y_j)} & \text{for}\quad i\neq j,\quad i,j=1,2,...,N_y,\\
-\sum_{\substack{j=1\\ i\neq j}}^{N_y}B_{ij}^{(1)} & \text{for}\quad i=j,\quad i,j=1,2,...,N_y
\end{cases}
\tag{58}
$$

In addition, the grid point distributions can be obtained as

$$
x_i=\frac{a}{2}\left[1-\cos\left(\frac{i-1}{N_x-1}\right)\pi\right]\qquad i=1,...,N_x
\tag{59}
$$

$$
y_i=\frac{b}{2}\left[1-\cos\left(\frac{i-1}{N_y-1}\right)\pi\right]\qquad i=1,...,N_y
\tag{60}
$$

Finally, the motion equations are given as matrix form as

$$
\left([K]\begin{Bmatrix}\{d_b\}\\ \{d_d\}\end{Bmatrix}+[C]\begin{Bmatrix}\{\dot d_b\}\\ \{\dot d_d\}\end{Bmatrix}+[M]\begin{Bmatrix}\{\ddot d_b\}\\ \{\ddot d_d\}\end{Bmatrix}\right)=\begin{Bmatrix}\{0\}\\ -Ma(t)\end{Bmatrix},
\tag{61}
$$

where the stiffness matrix is $[K]$, and the mass matrix and the damping matrix are $[M]$ and $[C]$, respectively. Also, domain points and boundaries are indicated by $\{d_d\}$ and $\{d_b\}$, respectively. Utilizing the Newmark method, Eq. (61) may be expressed as

$$
\begin{aligned}
&\left[K(d_{i+1})+\alpha_0 M+\alpha_1 C\right](d_{i+1})=\\
&\begin{bmatrix}Q_{i+1}+M\left(\alpha_0 d_i+\alpha_2\dot d_i+\alpha_3\ddot d_i\right)\\ +C\left(\alpha_1 d_i+\alpha_4\dot d_i+\alpha_5\ddot d_i\right)\end{bmatrix},
\end{aligned}
\tag{62}
$$

the subscript *i+1* denotes the time $t = t_{i+1}$ and

$$\alpha_0 = \frac{1}{\chi \Delta t^2}, \quad \alpha_1 = \frac{\gamma}{\chi \Delta t}, \quad \alpha_2 = \frac{1}{\chi \Delta t},$$
$$\alpha_3 = \frac{1}{2\chi} - 1, \quad \alpha_4 = \frac{\gamma}{\chi} - 1,$$
$$\alpha_5 = \frac{\Delta t}{2}\left(\frac{\gamma}{\chi} - 2\right), \quad , \alpha_6 = \Delta t\left(1 - \gamma\right), \tag{63}$$
$$\alpha_7 = \Delta t\, \gamma,$$

where $\gamma = 0.5$ and $\chi = 0.25$. Adopting the iteration method, the Eqs. (62) are solved at any time step and so acceleration vectors and velocity vectors which are modified can be defined as:

$$\ddot{d}_{i+1} = \alpha_0 (d_{i+1} - d_i) - \alpha_2 \dot{d}_i - \alpha_3 \ddot{d}_i, \tag{64}$$

$$\dot{d}_{i+1} = \dot{d}_i + \alpha_6 \ddot{d}_i + \alpha_7 \ddot{d}_{i+1}, \tag{65}$$

The above procedures should be repeated for all time steps to plot the deflection of the structure with respect to time.

4. Numerical example and discussion

For the parametric study, a pad concrete foundation with Poisson's ratio of $\nu_c = 0.3$ and elastic modulus of $E_c = 20\, GPa$ is assumed. The reinforcement is SiO_2 nanoparticles which the Poisson's ratio is $\nu_r = 0.2$ and elastic modulus is $E_r = 70\, GPa$. The smart layer is made from polyvinylidene fluoride (PVDF) in which the mechanical properties are expressed in Table 1 (Kolahchi *et al.* 2016).
The location of the study is Cheshme Sabs station of Bam with the axial, lateral and transverse accelerations shown in Figs. 2(a)-2(c).

Table 1 PVDF material properties

Properties	PVDF	
C_{11}	238.24	(GPa)
C_{12}	3.98	(GPa)
C_{22}	23.6	(GPa)
e_{11}	-0.135	(C/m^2)
e_{12}	-0.145	(C/m^2)
$\in_{11}$	1.1e-8	(C^2/Nm^2)

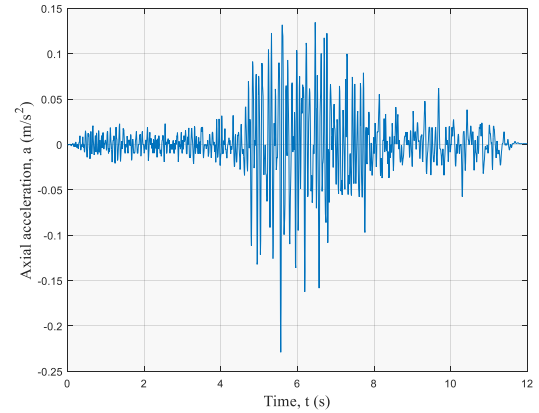

(a)

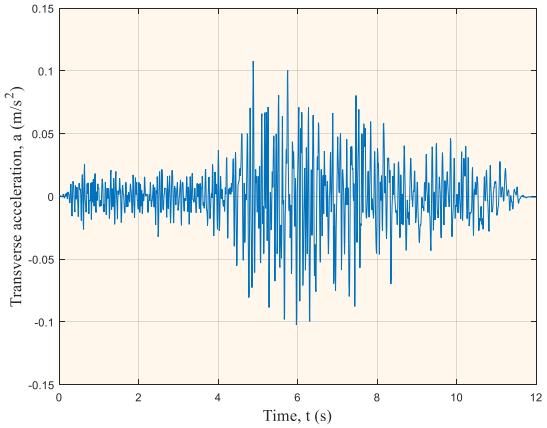

(b)

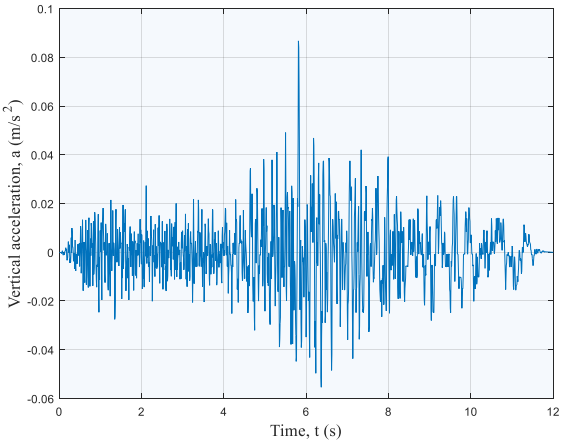

(c)

Fig. 2 Bam-Cheshme sabs station (a) axial acceleration (b) Transverse acceleration (c) Vertical acceleration of

4.1 Validation

Since there is not any work for molecular dynamic (MD) and experimental analysis of thick plates with piezoelectric layer under concentrated force, we neglected from nanoparticles in the plate, smart layer and soil foundation. However, we assumed a thick plated with uniform load

omitting the Kronecker product in Eq. (32). For validation, a plate with $h=0.138\ in$, $L_x=L_y=12\ in$, $\nu_{12}=0.32$, $G_{12}=G_{13}=G_{23}=0.37\times10^6\ psi$, $E_1=3\times10^6\ psi$, $E_2=1.28\times10^6\ psi$ is assumed. As demonstrated in Fig. 3, the results can be compared with the numerical results reported by Shen (2000), Zaghloul that used the classic plate theory (CPT) (1975), experiment results which declared by Zaghloul and Kennedy (1975) and Lei *et al*. (2013). The present results in this paper are close to the results which are presented by Lei *et al*. (2013) and Zaghloul and Kennedy (1975). Thus, the present results have a good agreement with experimental results.

In order to validate the results related to dynamic behavior, the dynamic deflection is obtained by supposing the nanoparticles are absent ($C_r=0$) and the smart layer. Thus, the mechanical characteristics and loadings are as the reference considered. As depicted in Fig. 4, the present numerical results are in accord with the corresponding references.

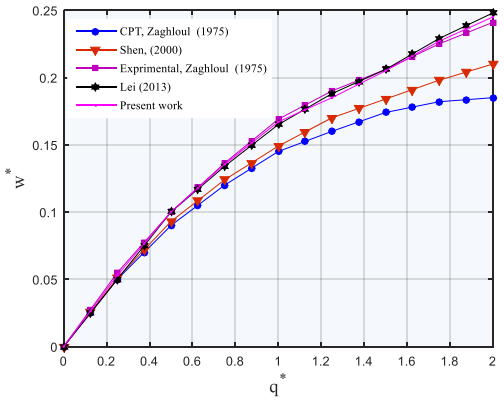

Fig. 3 Static transverse deflection of a simply supported plate under transverse load

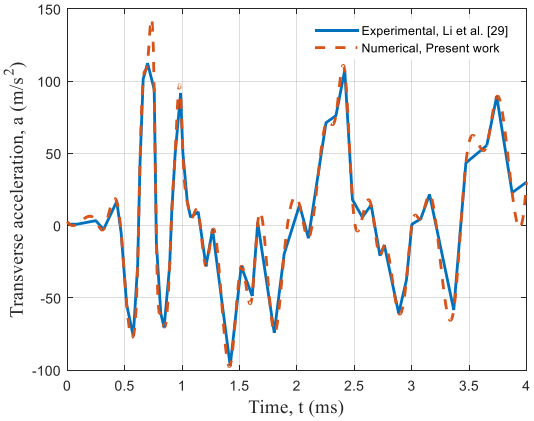

Fig. 4 The validation of this work with other works

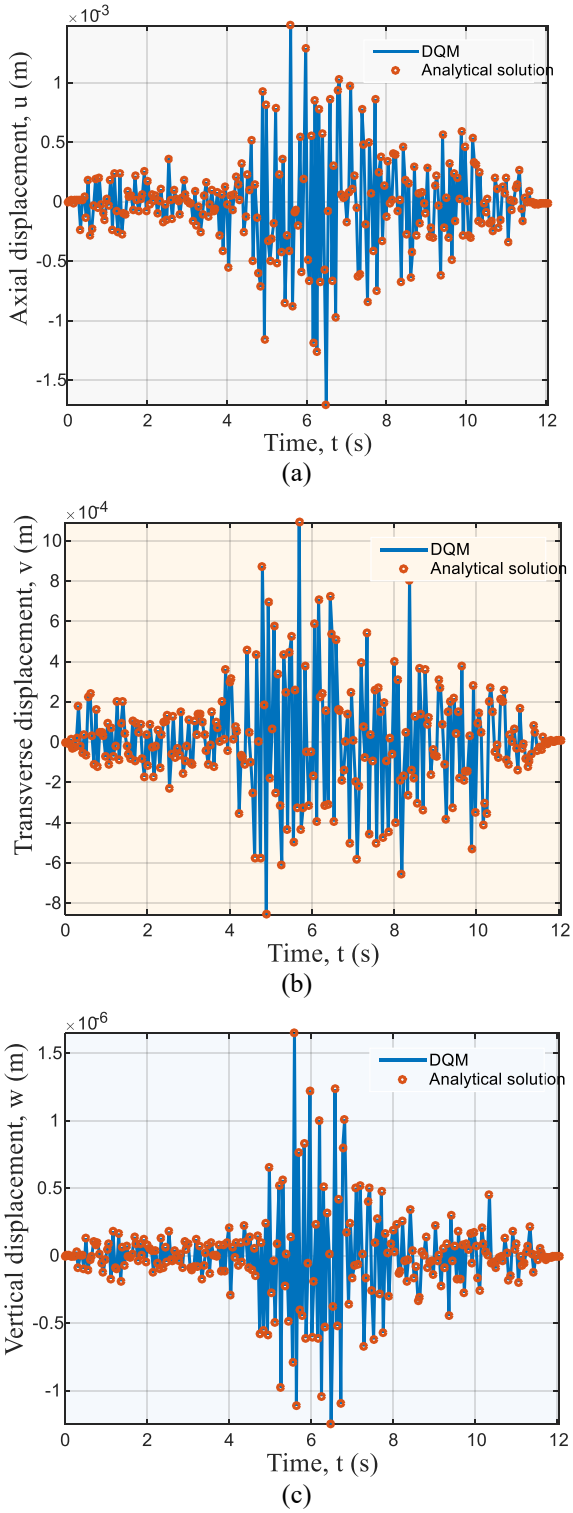

Fig. 5 Comparison of DQM and analytical method for (a) axial deflection (b) transverse deflection (c) vertical deflection

For another validation, the governing equations are solved by the DQM and analytical method of Navier. The dynamic deflection with respect to time is shown in Figs. 5(a)-5(c). Another validation can be inferred by the close results of the two solution methods.

Table 2 Convergence and accuracy of DQM

$N=Nx=N_y$	Axial deflection	Transverse deflection	Vertical deflection
7	5.32e-2	28.12e-4	8.58e-5
9	4.17e-3	15.43e-4	4.17e-6
11	2.01e-3	11.15e-4	2.72e-6
13	1.44e-3	10.19e-4	1.53e-6
15	1.48e-3	10.21e-4	1.58e-6
17	1.48e-3	10.21e-4	1.58e-6

4.2 Convergence of DQM

The convergence and accuracy of the numerical method for maximum dynamic deflection of the structure is presented in Table 1. As can be seen, in N=15, the results will be converged.

4.3 Effects of different parameters

Figs. 6(a)-6(c) illustrate that the silica nanoparticles volume percent have an effect on the axial, transverse and vertical dynamic deflections of the concrete structure, respectively. It is observed that with enhancing the silica nanoparticles volume percent, the dynamic deflection is decreased which is the result of the fact that as the silica nanoparticles increased the stiffness of structure increased. For example, the maximum dynamic displacement for the concrete foundation without nanoparticles is 2.5 mm while it is about 0.5 mm for pad concrete foundation containing 2% nanoparticles. It means a reduction of 80% in the dynamic displacement using SiO_2 nanoparticles in the foundation which is very remarkable. However, it may be concluded that using nanotechnology for reinforcing concrete foundations has an important role in improving the dynamic behavior of the model under the earthquake load.
Figs. 7(a)-7(c) show the influence of the agglomeration of silica nanoparticles on the axial, transverse and vertical dynamic deflections of the concrete structure, respectively. It can be concluded that consideration of the agglomeration of SiO_2 reinforcement leads to higher dynamic deflection about 50%. It is because the agglomeration of SiO_2 reinforcement decreases the stability and homogeneity of the model.
The effect of the applied voltage to the piezoelectric layer on the axial, transverse and vertical dynamic deflections of the concrete structure, respectively is shown in Figs. 8(a)-8(c). It can be concluded that by applying negative voltage to the smart layer, the dynamic deflection is reduced and with imposing positive one, the dynamic displacement is increased. It is physically due to this reason that applying a negative and positive voltage induces compressive and tensile loads in the structure. Form this figure it can be found that the smart layer can be used for smart control of the concrete foundation under the seismic load.
The axial, transverse and vertical dynamic deflections of the pad concrete foundation with the smart layer are depicted in Figs. 9(a)-9(c), respectively for the various soil mediums.

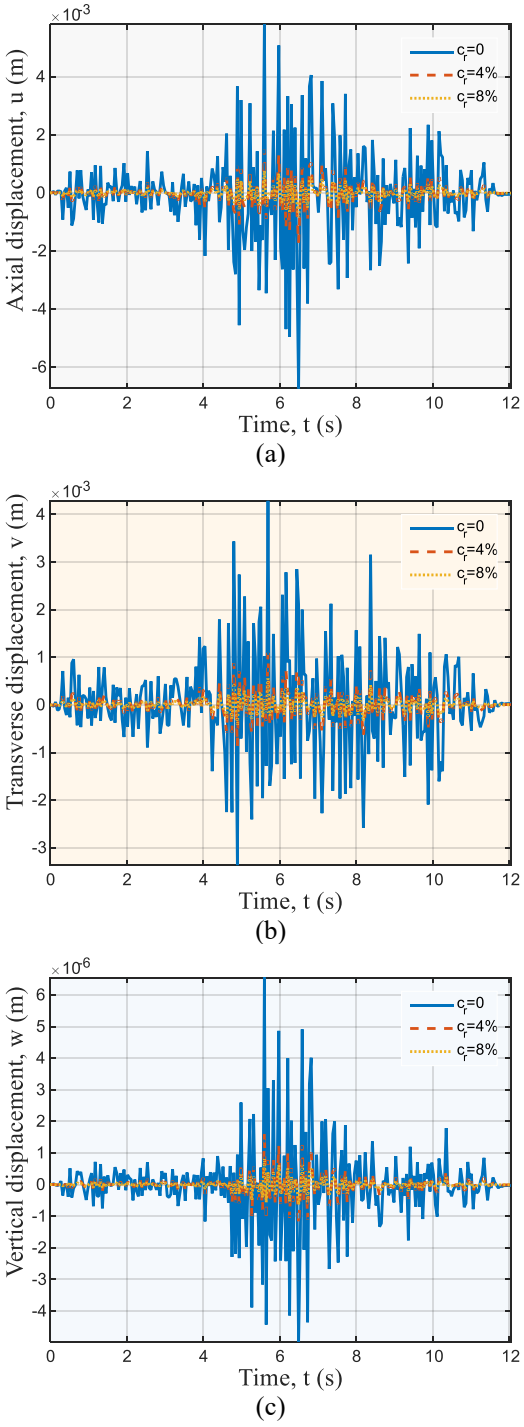

Fig. 6 The influence of the volume percent of silica nanoparticles on the (a) axial displacement (b) transverse displacement (c) vertical displacement

The figure shows, three cases of dense sand, and loose sand without soli medium are assumed. It is observed, the existence of soil medium decreases the dynamic behavior of the model. It is occurred according to consideration of soil medium which causes a stiffer the structure. Moreover, the dynamic deflection in the case of the soil medium with the dense sand is lower than the loose sand medium.

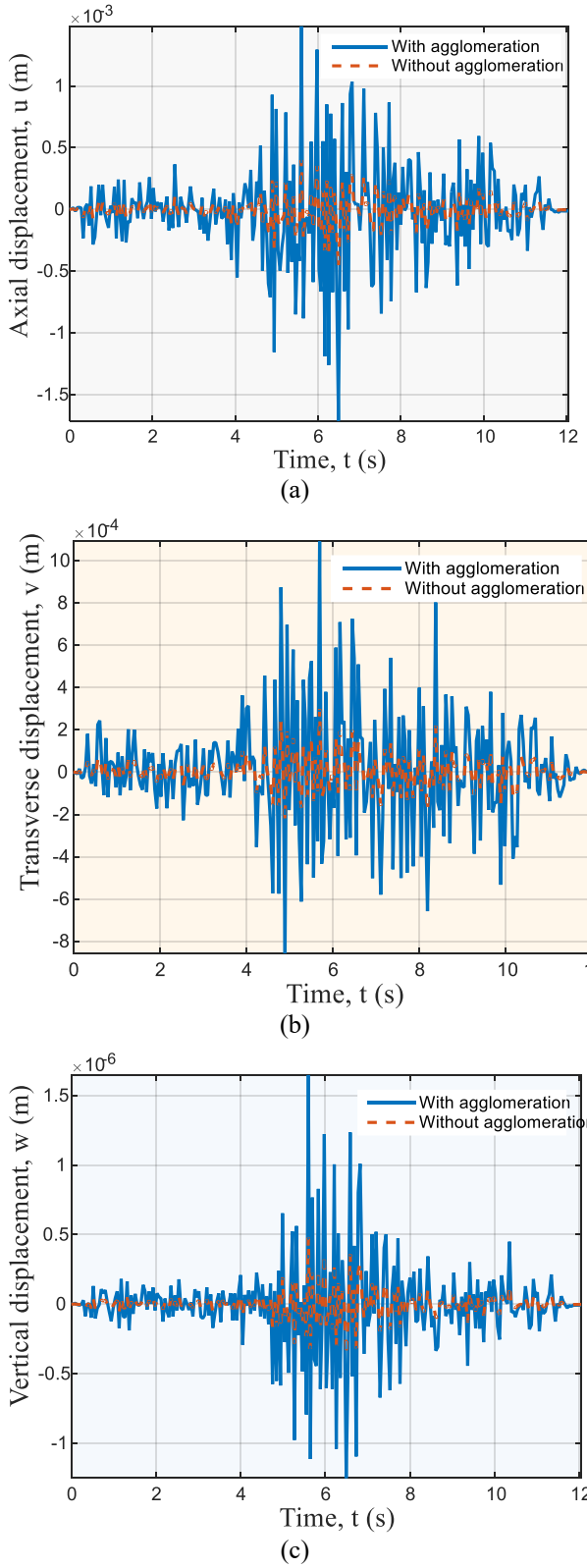

Fig. 7 The agglomeration of SiO_2 reinforcement effect on the (a) axial displacement (b) transverse displacement (c) vertical displacement

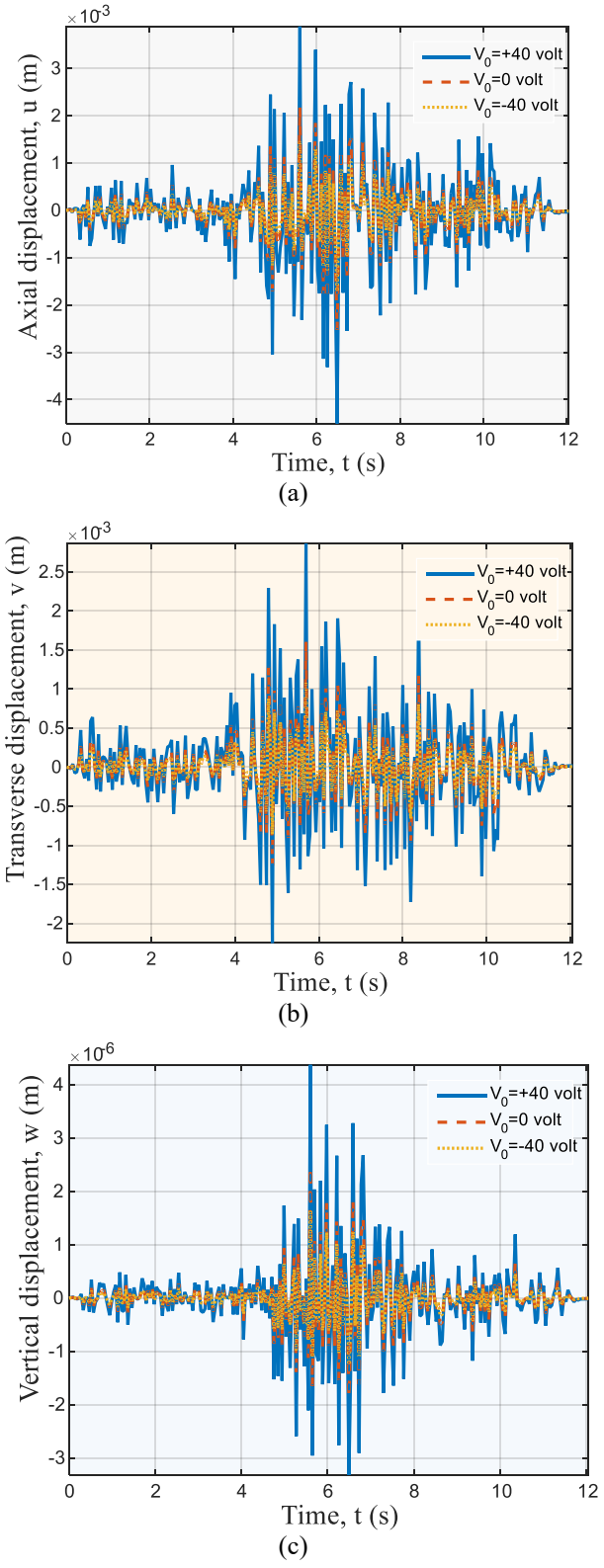

Fig. 8 The external voltage effect on the (a) axial displacement (b) transverse displacement (c) vertical displacement

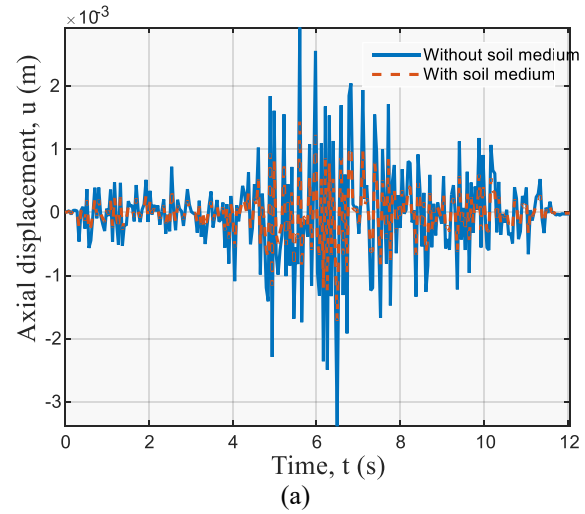

(a)

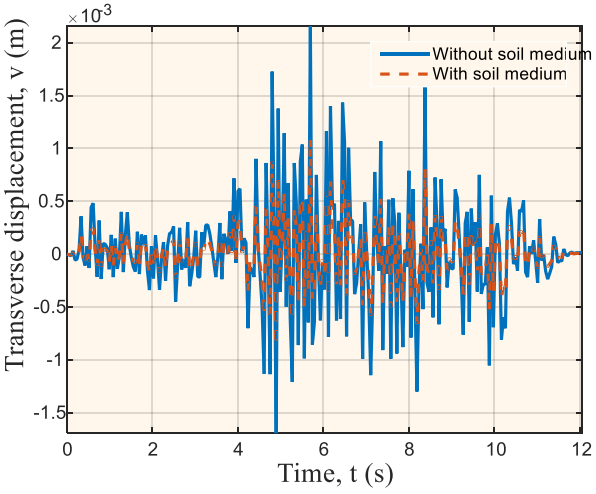

(b)

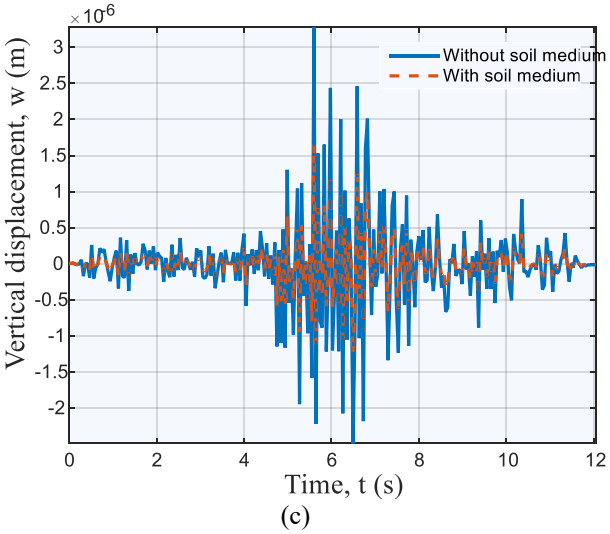

(c)

Fig. 9 The soil medium effect on the (a) axial displacement (b) transverse displacement (c) vertical displacement

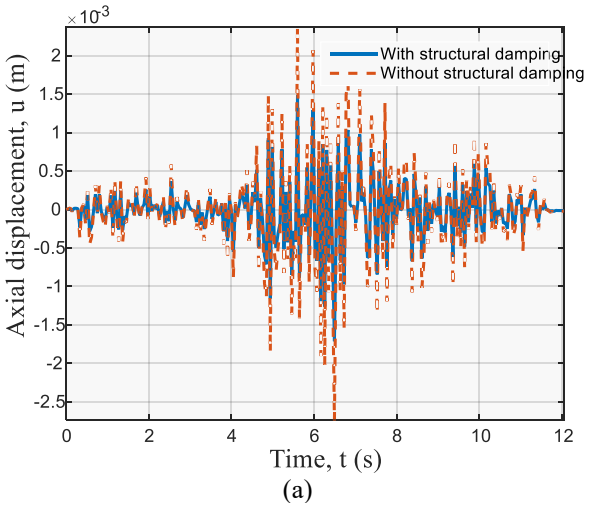

(a)

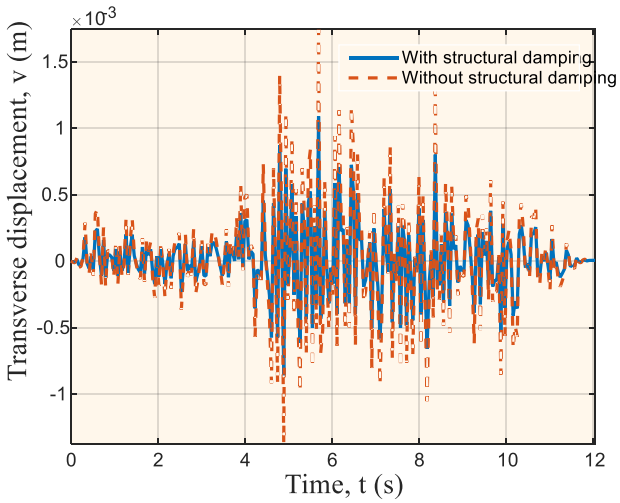

(b)

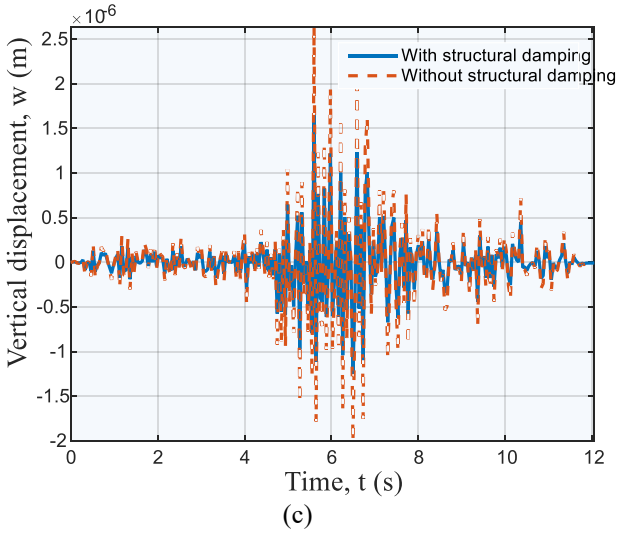

(c)

Fig. 10 The influence of structural damping on the (a) axial displacement (b) transverse displacement (c) vertical displacement

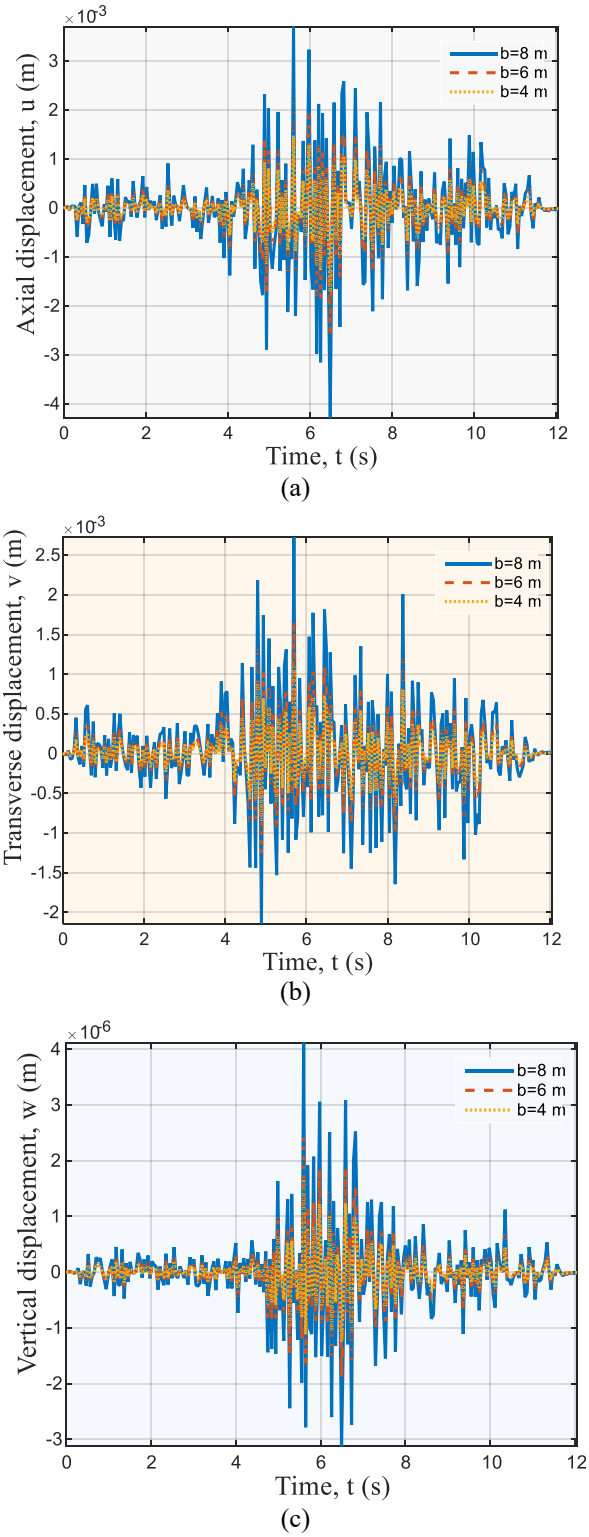

Fig. 11 The vertical dynamic response of the foundation on the (a) axial displacement (b) transverse displacement (c) vertical displacement

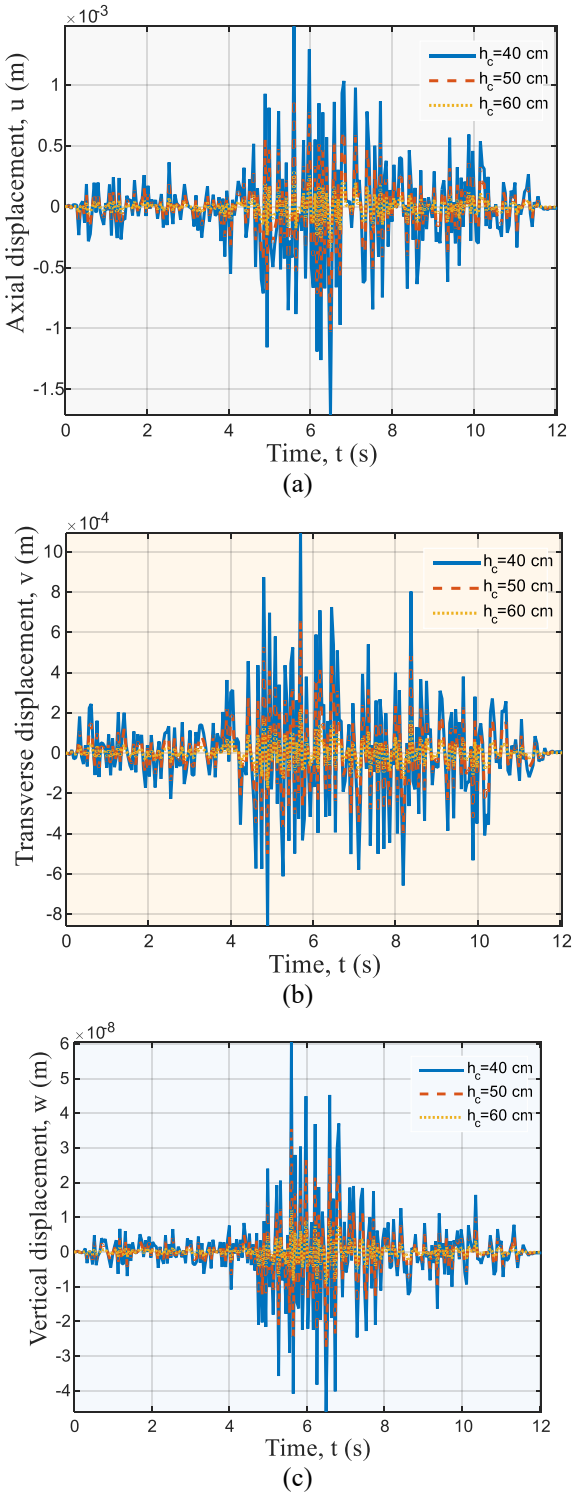

Fig. 12 The influence of the thickness of concrete foundation on the(a) axial displacement (b) transverse displacement (c) vertical displacement

The influence of the damping of structure on the axial, transverse and vertical dynamic deflections of the concrete structure, respectively is depicted in Figs. 10(a)-10(c). It is presented that by assuming the structural damping of the concrete structure, the dynamic deflection is reduced about 60%. Hence, for real modeling of the structure, assuming structural damping is essential.

Figs. 11(a)-11(c) and 12(a)-12(c) show the influence of width and thickness of the foundation on the dynamic deflection with respect to time of the earthquake, respectively. It can be found that the dynamic deflection is

decreased by enhancing the thickness and decreasing the width of the concrete foundation. It is since with decreasing the width and enhancing the thickness of the concrete foundation, the stiffness is reduced.

5. Conclusions

Dynamic deflection analysis in pad concrete foundation containing SiO_2 nanoparticles with a smart layer was presented in this research based on mathematical modeling. The weight load of the building was applied with a concentrated compressive load at the center of the foundation. The Mori-Tanaka and Kelvin-Voigt models were applied for modeling the nanoparticles in the foundation and structural damping, respectively. The governing equations were deduced by HSDT and Hamilton's principle. The methods of DQ and Newmark were used to calculate the dynamic response of the structure. The influence of the applied voltage, silica nanoparticles volume fraction and agglomeration, structural damping, soil medium and geometrical parameters of the concrete foundation were assessed. Results show that the maximum dynamic displacement for the concrete foundation without nanoparticles was 2.5 mm while it was about 0.5 mm for pad concrete foundation containing 2% nanoparticles. It means a reduction of 80% in the dynamic displacement using SiO_2 nanoparticles in the foundation. It can be concluded that consideration of the agglomeration of SiO_2 reinforcement leads to higher dynamic deflection about 50%. It was concluded that by applying negative voltage to the smart layer, the dynamic deflection is reduced and with imposing positive one, the dynamic displacement was increased. It was observed, the existence of soil medium decreases the dynamic behavior of the model. It was presented that by assuming the structural damping of the concrete structure, the dynamic deflection is reduced about 60%.

References

Amnieh, H.B., Zamzam, M.S. and Kolahchi, R. (2018), "Dynamic analysis of non-homogeneous concrete blocks mixed by SiO2 nanoparticles subjected to blast load experimentally and theoretically", *Constr. Build. Mater*., **174**, 633-644. DOI: 10.1016/j.conbuildmat.2018.04.140.

Azmi, M., Kolahchi, R. and Bidgoli, M.R. (2019), "Dynamic analysis of concrete column reinforced with Sio 2 nanoparticles subjected to blast load", *Adv. Concr. Constr*., **7**, 51-63. DOI: 10.12989/acc.2019.7.1.051.

Bilouei, B.S., Kolahchi, R. and Bidgoli, M.R. (2016), "Buckling of concrete columns retrofitted with Nano-Fiber Reinforced Polymer (NFRP)", *Comput. Concret*, 18, 1053–1063, DOI: https://doi.org/10.12989/cac.2016.18.6.1053

Duc, N.D. and Tung, H.V. (2011), "Mechanical and thermal postbuckling of higher order shear deformable functionally graded plates on elastic foundations"**,** Compos. Struct., **93**, 2874-2881,https://doi.org/10.1016/j.compstruct.2011.05.017.

Fakhar, M.H., Fakhar, A. and Tabatabaei, H. (2019), "Analysis of critical fluid velocity and heat transfer in temperature-dependent nanocomposite pipes conveying nanofluid subjected to heat generation, conduction, convection and magnetic field", *Steel Compos. Struct.,* 30, 281-292. DOI: https://doi.org/10.12989/scs.2019.30.3.281

Golabchi, H., Kolahchi, R. and Bidgoli, M.R. (2018), "Vibration and instability analysis of pipes reinforced by SiO2nanoparticles considering agglomeration effects", *Comput. Concr*., **21**, 431-440. https://doi.org/10.12989/cac.2018.21.4.431.

Haghighi, M.S., Keikha, R. and Heidari, A. (2018), "Dynamic analysis of immersion concrete pipes in water subjected to earthquake load using mathematical methods", *Earthq. Struct*., **15**, 361-367. DOI: 10.12989/eas.2018.15.4.361.

Hieu, P.T. and Tung, H.V. (2020), "Thermomechanical postbuckling of pressure-loaded CNT-reinforced composite cylindrical shells under tangential edge constraints and various temperature conditions", *Polym. Compos*., **41**, 244-257. https://doi.org/10.1002/pc.25365.

Hou, L., *et al*. (2019), "Effect of nanoparticles on foaming agent and the foamed concrete", *Constr. Build Mater*., **227**, 116698. DOI: 10.1016/j.conbuildmat.2019.116698.

Hajmohammad, M.H., Maleki, M. and Kolahchi, R. (2018), "Seismic response of underwater concrete pipes conveying fluid covered with nano-fiber reinforced polymer layer", *Soil Dyn. Earthq. Eng*., DOI: 10.1016/j.soildyn.2018.04.002.

Hosseini, P., *et al*. (2009), "Use of Nano-SiO2 to Improve Microstructure and Compressive Strength of Recycled Aggregate Concretes", *Nanotechnol. Construct.,* **3**, 215-221. DOI: 10.1007/978-3-642-00980-8_29.

Kargar, M. and Bidgoli, M.R. (2018), "Mathematical modeling of smart nanoparticles-reinforced concrete foundations: Vibration analysis", **27**(4), 465-477. *Steel Compos. Struct*., https://doi.org/10.12989/scs.2018.27.4.465.

Kolahchi, R., Hosseini, H. and Esmailpour, M. (2016), "Differential cubature and quadrature-Bolotin methods for dynamic stability of embedded piezoelectric nanoplates based on visco-nonlocal-piezoelasticity theories", *Compos. Struct.,* **157**, 174–186, https://doi.org/10.1016/j.compstruct.2016.08.032.

Lei, Z.X., Liew, K.M. and Yu, J.L. (2013), "Large deflection analysis of functionally graded carbon nanotubereinforced composite plates by the element-freekp-Ritz method", *Comput. Methods Appl. Mech. Eng.,* **256**, 189–199. DOI: https://doi.org/10.1016/j.cma.2012.12.007.

Lei, Z.X., Zhang, L.W. and Liew K.M. (2016), "Analysis of laminated CNT reinforced functionally graded plates using the element-free kp-Ritz method", *Compos. B. Eng*., **84**, 211-221, https://doi.org/10.1016/j.compositesb.2015.08.081.

Liew, K.M., Pan, Z.Z. and Zhnag, L.w. (2019), "An overview of layerwise theories for composite laminates and structures: Development, numerical implementation and application", *Compos. Struct*., **216**, 240-259., https://doi.org/10.1016/j.compstruct.2019.02.074.

Long, V.T. and Tung, H.V. (2019) "Thermomechanical postbuckling behavior of CNT-reinforced composite sandwich plate models resting on elastic foundations with elastically restrained unloaded edges", *Therm. Stress*., **42**, 658-682. https://doi.org/10.1080/01495739.2019.1571972.

Maleki, M. and Bidgoli, M.R. (2018), "Seismic response of underwater fluid-conveying concrete pipes reinforced with SiO2nanoparticles using DQ and Newmark methods", *Comput. Concr*., **21**, 717-726. https://doi.org/10.12989/cac.2018.21.6.717.

Maleki, M., Bidgoli, M.R. and Kolahchi, R. (2019), "Earthquake response of nanocomposite concrete pipes conveying and immersing in fluid using numerical methods", *Comput. Concret*., 24, 125-135. https://doi.org/10.12989/cac.2019.24.2.125.

Motezaker, M. and Kolahchi, R. (2017), "Seismic response of SiO2nanoparticles-reinforced concrete pipes based on DQ and newmark methods", *Comput. Concret*, **19**, 745-753. https://doi.org/10.12989/cac.2017.19.6.745.

Nouri, A.Z. (2017), "Mathematical modeling of concrete pipes reinforced with CNTs conveying fluid for vibration and stability analyses", *Comput. Concret*, **18**, 325-331. https://doi.org/10.12989/cac.2017.19.3.325.

Nouri, A.Z. (2018), "Seismic response of soil foundation surrounded Fe2O3 nanoparticles-reinforced concrete pipes conveying fluid", *Soil Dyn. Earthq. Eng*., 106, 53-59. DOI: 10.1016/j.soildyn.2017.12.009.

Pan, Z.Z., Zhang, L.W. and Liew, K.M. (2019), "Modeling geometrically nonlinear large deformation behaviors of matrix cracked hybrid composite deep shells containing CNTRC layers", *Comput. Method. Appl. M*., **355**, 753-778. https://doi.org/10.1016/j.cma.2019.06.04.

Reddy, J.N. (2002), *Mechanics of Laminated Composite Plates and Shells: Theory and Analysis*, Second Edition, CRC Press,.

Shen, H.S. (2000), "Nonlinear bending of shear deformable laminated plates under transverse and in-plane loads and resting on elastic foundations", *Compos. Struct*., **50**, 131–142. https://doi.org/10.1016/S0263-8223(00)00088-X.

Shi, D.L. and Feng, X.Q. (2004), "The Effect ofNanotube Waviness and Agglomeration on the Elastic Property of Carbon Nanotube-Reinforced Composties", *J. Eng. Mat. Tech. - ASME,* **126**, 250-270, DOI: https://doi.org/10.1115/1.1751182

Su, Y., *et al.* (2016), "Influences of nano-particles on dynamic strength of ultra-high performance concrete", *Compos. Part B Eng*., **91**, 595-609. DOI: 10.1016/j.compositesb.2016.01.044.

Sharifi, M., Kolahchi, R. and Bidgoli, M.R. (2018), "Dynamic analysis of concrete beams reinforced with Tio2nano particles under earthquake load", *Wind Struct.,* **26**(1), 1-9. https://doi.org/10.12989/was.2018.26.1.001.

Shokravi, M. (2017), "Vibration analysis of silica nanoparticles-reinforced concrete beams considering agglomeration effects", *Comput. Concret*., **19**(3), 333-338. https://doi.org/10.12989/cac.2017.19.3.333.

Tiersten, H.F. (1969), *Linear Piezoelectric Plate Vibrations, Plenum Press*, New York.

Tung, H.V. (2017), "Thermal buckling and postbuckling behaviour of functionally graded carbon-nanotube-reinforced composite plates resting on elastic foundations with tangential-edge restraints", *Therm. Stress*., **40**, 641-663. https://doi.org/10.1080/01495739.2016.1254577.

Tung, H.V. and Trang, L.T.N. (2020), "Thermal postbuckling of shear deformable CNT-reinforced composite plates with tangentially restrained edges and temperature-dependent properties", *J. Thermoplast. Compos. Mater*., **33**, 97-124. https://doi.org/10.1177/0892705718804588.

Younis, K.H. and Mustafa, S.M. (2018), "Feasibility of Using Nanoparticles of SiO 2 to Improve the Performance of Recycled Aggregate Concrete", *Adv. Mater. Sci. Eng.*, DOI: 10.1155/2018/1512830.

Zamani, A., Kolahchi, R. and Bidgoli, M.R. (2017), "Seismic response of smart nanocomposite cylindrical shell conveying fluid flow using HDQ-Newmark methods", *Comput. Concret*, **20**, 671-682. https://doi.org/10.12989/cac.2017.20.6.671.

Zarei, M.S., *et al*. (2017), "Seismic response of underwater fluid-conveying concrete pipes reinforced with SiO2nanoparticles and fiber reinforced polymer (FRP) layer", *Soil Dyn. Earthq. Eng*., **103**, 76-85. DOI: 10.1016/j.soildyn.2017.09.009.

Zaghloul, S.A. and Kennedy, J.B. (1975), "Nonlinear behavior of symmetrically laminated plates", *J. Appl. Mech. T. - ASME* **931**, 236-234. DOI: https://doi.org/10.1115/1.3423532.

Zhang, L.W., (2017), "Geometrically nonlinear large deformation of CNT-reinforced composite plates with internal column supports", *J. Model. Mech. Mater.*, **1**, https://doi.org/10.1515/jmmm-2016-0154.

Zhang, L.W., (2017), "On the study of the effect of in-plane forces on the frequency parameters of CNT-reinforced composite skew plates", *Compos. Struct*., **160**, 824-837. https://doi.org/10.1016/j.compstruct.2016.10.116.

Zhang, L.W. (2017), "An element-free based IMLS-Ritz method for buckling analysis of nanocomposite plates of polygonal planform", *Eng. Anal. Bound. Elem.*, **77**, 10-25. https://doi.org/10.1016/j.enganabound.2017.01.004.

Zhang, L.W., Liew, K.M. and Jiang Z. (2016), "An element-free analysis of CNT-reinforced composite plates with column supports and elastically restrained edges under large deformation", Compos. *B. Eng*., **95**, 18-28. https://doi.org/10.1016/j.compositesb.2016.03.078.

Zhang, L.W. and Liew, K.M. (2016), "Postbuckling analysis of axially compressed CNT reinforced functionally graded composite plates resting on Pasternak foundations using an element-free approach", *Compos. Struct.*, **15**, 40-51. https://doi.org/10.1016/j.compstruct.2015.11.031.

Zhang, L.W. and Liew, K.M. (2016), "Element-free geometrically nonlinear analysis of quadrilateral functionally graded material plates with internal column supports", *Compos. Struct.*, **147**, 99-110. https://doi.org/10.1016/j.compstruct.2016.03.034.

Zhang, L.W., Liew, K.M. and Reddy J.N. (2016), "Postbuckling of carbon nanotube reinforced functionally graded plates with edges elastically restrained against translation and rotation under axial compression", *Comput Method. Appl M.*, **298**, 1-28. https://doi.org/10.1016/j.cma.2015.09.016.

Zhang, L.W., Liew, K.M. and Reddy J.N. (2016), "Postbuckling analysis of bi-axially compressed laminated nanocomposite plates using the first-order shear deformation theory", *Compos. Struct*., **152**, 418-431. https://doi.org/10.1016/j.compstruct.2016.05.040.

Zhang, L.W., Liew, K.M. and Reddy J.N. (2016), "Postbuckling behavior of bi-axially compressed arbitrarily straight-sided quadrilateral functionally graded material plates", *Comput Method. Appl Mech Eng. Compos. Struct*., **300**, 593-610. https://doi.org/10.1016/j.cma.2015.11.030.

Zhang, L.W., Liu, W.H. and Liew, K.M. (2016), "Geometrically nonlinear large deformation analysis of triangular CNT-reinforced composite plates", *Int. J. Nonlin. Mech*., **86**, 122-132. https://doi.org/10.1016/j.ijnonlinmec.2016.08.004.

Zhang, L.W. and Selim, B.A. (2017), "Vibration analysis of CNT-reinforced thick laminated composite plates based on Reddy's higher-order shear deformation theory", *Compos. Struct*., **160**, 689-705. https://doi.org/10.1016/j.compstruct.2016.10.102.

Zhang, L.W., Song, Z.G. and Liew, K.M. (2016), "Optimal shape control of CNT reinforced functionally graded composite plates using piezoelectric patches", *Compos. B. Eng*., **85**, 140-149. https://doi.org/10.1016/j.compositesb.2015.09.044.

Zhang, L.W., Song, Z.G. and Liew, K.M. (2016), "Computation of aerothermoelastic properties and active flutter control of CNT reinforced functionally graded composite panels in supersonic airflow", *Comput Method. Appl. M.*, **300**, 427-441. https://doi.org/10.1016/j.cma.2015.11.029.

Zhang, L.W., Song, Z.G., Qiao P. and Liew, K.M. (2017), "Modeling of dynamic responses of CNT-reinforced composite cylindrical shells under impact loads", *Comput Method. Appl. M*., **313**, 889-903. https://doi.org/10.1016/j.cma.2016.10.020.

Zhang, L.W. and Xiao, L.N. (2017), "Mechanical behavior of laminated CNT-reinforced composite skew plates subjected to dynamic loading", *Compos. B. Eng*., **122**, 219-230. https://doi.org/10.1016/j.compositesb.2017.03.041.

Zhang, L.W., Xiao, L.N., Zou, G.L. and Liew, K.M. (2016), "Elastodynamic analysis of quadrilateral CNT-reinforced functionally graded composite plates using FSDT element-free method", *Compos. Struct.*, **148**, 144-154. https://doi.org/10.1016/j.compstruct.2016.04.006.

Zhang, L.W., Zhang, Y., Zou, G.L. and Liew, K.M. (2016), "Free

vibration analysis of triangular CNT-reinforced composite plates subjected to in-plane stresses using FSDT element-free method", *Compos. Struct*., **149**, 247-260. https://doi.org/10.1016/j.compstruct.2016.04.019.

Zhang, M. and Yu, S. (2011), "Impact property of concrete containing nano-particles for pavement", *Adv. Mat. Res*., **33**, 417-420. DOI: 10.4028/www.scientific.net/AMR.250-253.417.

CC

Appendix A

$$K = K_{out}\left[1+\frac{\xi\left(\frac{K_{in}}{K_{out}}-1\right)}{1+\frac{\left(1+\frac{3K_{out}-2G_{out}}{6K_{out}+2G_{out}}\right)}{3\left(1-\frac{3K_{out}-2G_{out}}{6K_{out}+2G_{out}}\right)}(1-\xi)\left(\frac{K_{in}}{K_{out}}-1\right)}\right], \tag{A1}$$

$$G = G_{out}\left[1+\frac{\xi\left(\frac{G_{in}}{G_{out}}-1\right)}{1+\frac{2\left(4-5\frac{3K_{out}-2G_{out}}{6K_{out}+2G_{out}}\right)}{15\left(1-\frac{3K_{out}-2G_{out}}{6K_{out}+2G_{out}}\right)}(1-\xi)\left(\frac{G_{in}}{G_{out}}-1\right)}\right], \tag{A2}$$

where

$$K_{in} = K_m + \frac{\left(\delta_r - 3K_m\chi_r\right)C_r\zeta}{3\left(\xi - C_r\zeta + C_r\zeta\chi_r\right)}, \tag{A3}$$

$$K_{out} = K_m + \frac{C_r\left(\delta_r - 3K_m\chi_r\right)(1-\zeta)}{3\left[1-\xi-C_r(1-\zeta)+C_r\chi_r(1-\zeta)\right]}, \tag{A4}$$

$$G_{in} = G_m + \frac{\left(\eta_r - 3G_m\beta_r\right)C_r\zeta}{2\left(\xi - C_r\zeta + C_r\zeta\beta_r\right)}, \tag{A5}$$

$$G_{out} = G_m + \frac{C_r\left(\eta_r - 3G_m\beta_r\right)(1-\zeta)}{2\left[1-\xi-C_r(1-\zeta)+C_r\beta_r(1-\zeta)\right]}, \tag{A6}$$

where $\delta_r, \chi_r, \eta_r, \beta_r$ can be determined as

$$\chi_r = \frac{3\left(K_m + G_m\right) + k_r - l_r}{3\left(k_r + G_m\right)}, \tag{A7}$$

$$\beta_r = \frac{1}{5}\left\{\begin{array}{l}\frac{4G_m + 2k_r + l_r}{3\left(k_r + G_m\right)} + \frac{4G_m}{\left(p_r + G_m\right)} \\ + \frac{2\left[G_m\left(3K_m + G_m\right) + G_m\left(3K_m + 7G_m\right)\right]}{G_m\left(3K_m + G_m\right) + m_r\left(3K_m + 7G_m\right)}\end{array}\right\}, \tag{A8}$$

$$\delta_r = \frac{1}{3}\left[n_r + 2l_r + \frac{\left(2k_r - l_r\right)\left(3K_m + 2G_m - l_r\right)}{k_r + G_m}\right], \tag{A9}$$

$$\eta_r = \frac{1}{5}\left[\begin{array}{l}\frac{2}{3}\left(n_r - l_r\right) + \frac{4G_m p_r}{\left(p_r + G_m\right)} \\ + \frac{8G_m m_r\left(3K_m + 4G_m\right)}{3K_m\left(m_r + G_m\right) + G_m\left(7m_r + G_m\right)} \\ + \frac{2\left(k_r - l_r\right)\left(2G_m + l_r\right)}{3\left(k_r + G_m\right)}\end{array}\right]. \tag{A10}$$

where, the bulk modulus (K_m) and shear modulus (G_m) o f the matrix are defined as:

$$K_m = \frac{E_m}{3\left(1-2\upsilon_m\right)}, \tag{A11}$$

$$G_m = \frac{E_m}{2\left(1+\upsilon_m\right)}. \tag{A12}$$

In above relations, C_m is the volume fractions of the m atrix and C_r is the the volume fractions of nanoparticles respectively and ξ and ζ describe the agglomeration of nanoparticles.

Appendix B

$$
\begin{aligned}
&A_{110}\frac{\partial^2 u}{\partial x^2}+A_{111}\frac{\partial^2 \phi_x}{\partial x^2}+A_{120}\frac{\partial^2 v}{\partial y\,\partial x}\\
&+A_{121}\frac{\partial^2 \phi_y}{\partial y\,\partial x}+E_{31}\frac{\partial \varphi}{\partial x}+A_{120}\frac{\partial^2 u}{\partial x\,\partial y}\\
&+A_{121}\frac{\partial^2 \phi_x}{\partial x\,\partial y}+A_{220}\frac{\partial^2 v}{\partial y^2}+A_{221}\frac{\partial^2 \phi_y}{\partial y^2}\\
&+E_{32}\frac{\partial \varphi}{\partial y}=I_0\frac{\partial^2 u}{\partial t^2}+I_1\frac{\partial^2 \phi_x}{\partial t^2},
\end{aligned}
\tag{B1}
$$

$$
\begin{aligned}
&A_{120}\frac{\partial^2 u}{\partial x\,\partial y}+A_{121}\frac{\partial^2 \phi_x}{\partial x\,\partial y}+A_{220}\frac{\partial^2 v}{\partial y^2}\\
&+A_{221}\frac{\partial^2 \phi}{\partial y^2}+E_{32}\frac{\partial \varphi}{\partial y}+A_{660}\left(\frac{\partial^2 u}{\partial y\,\partial x}+\frac{\partial^2 v}{\partial x^2}\right)\\
&+A_{661}\left(\frac{\partial^2 \phi_x}{\partial y\,\partial x}+\frac{\partial^2 \phi_y}{\partial x^2}\right)=I_0\frac{\partial^2 v}{\partial t^2}+I_1\frac{\partial^2 \phi_y}{\partial t^2},
\end{aligned}
\tag{B2}
$$

$$
\begin{aligned}
&k'A_{44}\left[\frac{\partial w}{\partial y^2}+\frac{\partial \phi_y}{\partial y}\right]+E_{15}\frac{\partial \varphi}{\partial y^2}\\
&+k'A_{55}\left(\frac{\partial^2 w}{\partial x^2}+\frac{\partial \phi_x}{\partial x}\right)+E_{24}\frac{\partial^2 \varphi}{\partial x^2}-\\
&A_{120}\frac{\partial u}{\partial x}-A_{121}\frac{\partial \phi_x}{\partial x}-A_{220}\left(\frac{\partial v}{\partial y}\right)-A_{221}\frac{\partial \phi}{\partial y},
\end{aligned}
\tag{B3}
$$

$$
\begin{aligned}
&N^f_{xx}\frac{\partial^2 w}{\partial x^2}+N^f_{yy}\frac{\partial^2 w}{\partial y^2}-F\delta(x-a/2)(y-b/2)\\
&-K_s w=I_0\frac{\partial^2 w}{\partial t^2}+\mathrm{ma},
\end{aligned}
$$

$$
\begin{aligned}
&A_{111}\frac{\partial^2 u}{\partial x^2}+A_{112}\frac{\partial^2 \phi_x}{\partial x^2}+A_{121}\left(\frac{\partial^2 v}{\partial y\,\partial x}+\frac{\partial w}{\partial x}\right)\\
&+A_{122}\frac{\partial^2 \phi_y}{\partial y}+F_{31}\frac{\partial \phi}{\partial x}+A_{661}\left(\frac{\partial^2 u}{\partial y^2}+\frac{\partial^2 v}{\partial x\,\partial y}\right)\\
&+A_{662}\left(\frac{\partial^2 \phi_x}{\partial y^2}+\frac{\partial^2 \phi_y}{\partial x\,\partial y}\right)-k'A_{55}\left(\frac{\partial w}{\partial x}+\phi_x\right)\\
&-E_{24}\frac{\partial \varphi}{\partial x}=I_2\frac{\partial^2 \phi_x}{\partial t^2}+I_1\frac{\partial^2 u}{\partial t^2},
\end{aligned}
\tag{B4}
$$

$$
\begin{aligned}
&A_{121}\frac{\partial^2 u}{\partial x\,\partial y}+A_{122}\frac{\partial^2 \phi_x}{\partial x\,\partial y}+A_{221}\left(\frac{\partial^2 v}{\partial y^2}+\frac{\partial w}{\partial y}\right)\\
&+A_{222}\frac{\partial^2 \phi_y}{\partial y^2}+F_{32}\frac{\partial \varphi}{\partial y}+A_{661}\left(\frac{\partial^2 u}{\partial y\,\partial x}+\frac{\partial^2 v}{\partial x^2}\right)\\
&+A_{662}\left(\frac{\partial^2 \phi_x}{\partial y\,\partial x}+\frac{\partial^2 \phi_y}{\partial x^2}\right)-k'A_{44}\left[\frac{\partial w}{\partial y}+\phi_y\right]\\
&-E_{15}\frac{\partial \varphi}{\partial y}=I_2\frac{\partial^2 \phi_y}{\partial t^2}+I_1\frac{\partial^2 v}{\partial t^2},
\end{aligned}
\tag{B5}
$$

$$
\begin{aligned}
&\delta\phi:\ -E_{15}\left(\frac{\partial \phi_x}{\partial x}+\frac{\partial^2 w}{\partial x^2}\right)+\Xi_{11}\left(\frac{\partial^2 \varphi}{\partial x\,\partial y}\right)\\
&-E_{24}\left(\frac{\partial^2 w}{\partial y^2}+\frac{\partial \phi_y}{\partial y}\right)+\Xi_{22}\left(\frac{\partial^2 \varphi}{\partial y^2}\right)+E_{31}\frac{\partial u}{\partial x}\\
&+F_{31}\frac{\partial \phi_x}{\partial x}+\frac{E_{32}}{R}\left(w+\frac{\partial v}{\partial y}\right)+F_{32}\frac{\partial \phi_y}{\partial y}-\Xi_{33}\varphi=0.
\end{aligned}
\tag{B6}
$$

where

$$
(\Xi_{11},\Xi_{22})=\int_{-h/2}^{h/2}(\in_{11},\in_{22})\cos^2\left(\frac{\pi z}{h}\right)dz, \tag{B7}
$$

$$
(\Xi_{33})=\frac{\pi^2}{h^2}\int_{-h/2}^{h/2}(\in_{33})\sin^2\left(\frac{\pi z}{h}\right)dz. \tag{B8}
$$